TECHNISCHE UNIVERSITÄT WIEN
Vienna University of Technology

INSTITUT FÜR MECHANIK UND MECHATRONIK
Mechanics & Mechatronics

Diploma Thesis

Design of a Nonlinear Multivariable Model-Based Control Strategy for a Recombinant Protein Production Process in *C. glutamicum*

carried out for the purpose of obtaining the degree of Master of Science (MSc or Dipl.-Ing. or DI) under the supervision of

Univ. Prof. Dipl.-Ing. Dr. Stefan Jakubek

Institute of Mechanics and Mechatronics

submitted at TU Wien, Faculty of Mechanical and Industrial Engineering, by

Johanna Bartlechner

Mat.Nr.: 01426999

Vienna, March 31, 2022

Johanna Bartlechner

I confirm, that going to press of this thesis needs the confirmation of the examination committee.

Affidavit

I declare in lieu of oath, that I wrote this thesis and performed the associated research myself, using only literature cited in this volume. If text passages from sources are used literally, they are marked as such.

I confirm that this work is original and has not been submitted elsewhere for any examination, nor is it currently under consideration for a thesis elsewhere.

I acknowledge that the submitted work will be checked electronicallytechnically using suitable and state-of-the-art means (plagiarism detection software). On the one hand, this ensures that the submitted work was prepared according to the high-quality standards within the applicable rules to ensure good scientific practice "Code of Conduct" at the TU Wien. On the other hand, a comparison with other student theses avoids violations of my personal copyright.

Vienna, March 31, 2022 Johanna Bartlechner

Acknowledgment

Throughout the writing of this thesis I have received a great deal of support and assistance.

I would first like to thank my supervisor, Professor Stefan Jakubek, whose intellectual guidance was invaluable. Your insightful feedback pushed me to sharpen my thinking and brought my work to a higher level.

Furthermore, I would like to thank Professor Christoph Herwig for his professional expertise, without whom this interdisciplinary work would not have been possible. Your regular feedback and annotations made a crucial contribution towards the improvement of the thesis.

I would like to acknowledge the research team in whose theoretical and practical activities this work is embedded. Daniel Waldschitz, Peter Sinner, Julian Kager, Bence Kozma, Eva Karner, Yannick Bus, Jakob Kitzmüller and Mathias Petsch - a special thank you to all of you and your relentless and qualitative work ethic as well as collegial environment.

In addition, I would like to thank my partner, friends and fellow students, with whom I have gone through the demanding, challenging, interesting and fascinating phases of my studies. I am very grateful for the sympathetic ear, the inspiring discussions and the positive encouragement.

And finally, I would like to express my gratitude towards my family. Their intellectual curiosity, persistence, perseverance and inexhaustibility have always been an inspiration. My gratefulness is beyond measure and truly tremendous.

Abstract

Linear economics and the generation of many by- and waste products in huge quantities contribute to a resource inefficient and environmentally harmful economy. By recycling sulfide spend liquor (SSL), a waste stream from the pulp mill process, and spruce hydrolysate, a byproduct from Borregaards advanced lignin process (BALI™), as alternative carbon sources for bioprocessing, the development of more sustainable and economical processes is further pushed. However, due to complex composition and possible inhibitory effects, bioprocessing on SSL and BALI™ is, despite their high sugar concentrations, challenging. Therefore, advanced model-based approaches for both process understanding and process control are needed to ensure reproducible, efficient and stable processes.

In this thesis, a model-based control strategy is designed with the method of feedback linearization. A process model and parameter-set derived from recent literature are used to examine the suitability of process control of a continuous bioprocess with cell retention. *C. glutamicum* is processed with SSL, BALI™ and a nutrient solution. The novelty of this thesis is the design, implementation and testing of a nonlinear model-based control strategy with state estimation that enables the control of biomass, sugar and nutrient concentration as well as the volume by adapting three feeds, harvest rate and bleed rate while minimizing measurement expenses.

Within a feasibility study, possible setpoints as well as physical and biochemical limitations are shown. The influence of process parameters on the resulting control law is examined in a robustness analysis. Two different control strategies based on the feedback linearized system, a feedforward controller and a model predictive controller (MPC) including a state observer, are proposed and analysed. It can be seen, that the control of the biological states with two independent carbon-sources enables the possibility to control the process in a dynamic way. By choosing different setpoints, the ratio between the added SSL and BALI™ can be influenced. Especially when the concentrations in the feeds vary, the suggested control strategies show their potential - by adapting the input variables of the process accordingly, a stable state can be maintained.

Kurzfassung

Lineare Produktionsprozesse und die Erzeugung vieler Neben- und Abfallprodukte in großen Mengen tragen zu einer ressourcenineffizienten und umweltschädlichen Wirtschaft bei. Der Einsatz alternativer Kohlenstoffquellen, wie Sulfidablauge (SSL) und Fichtenhydrolysat, ein Nebenprodukt aus Borregaards fortschrittlichem Ligninprozess (BALI™), ermöglicht die Entwicklung nachhaltiger und wirtschaftlicher Bioprozesse. Aufgrund komplexer Zusammensetzung und möglicher hemmender Inhaltsstoffe ist die biologische Verarbeitung von SSL und BALI™ eine Herausforderung. Es werden fortschrittliche modellbasierte Ansätze sowohl für das Prozessverständnis als auch für die Prozesssteuerung benötigt, um reproduzierbare, effiziente und stabile Prozesse zu gewährleisten.

In dieser Arbeit wird eine modellbasierte Regelungsstrategie mit der Methode der Feedback Linearisierung entworfen. Ein Prozessmodell und Parametersatz aus der Literatur werden verwendet um den kontinuierlichen Prozess mit Zellrückhaltung zu beschreiben. *C. glutamicum* wird mit SSL, BALI™ und einer Nährlösung fermentiert. Die Forschungslücke, welcher sich in der Arbeit angenommen wird, ist der Entwurf und die Implementierung einer nicht linearen modellbasierten Regelungsstrategie mit Zustandsschätzung, welche die Regelung der Biomasse-, Zucker-, Nährstoffkonzentration und des Volumens durch Anpassung der Zu- und Abläufe bei gleichzeitiger Minimierung des Messaufwands ermöglicht.

Mögliche Sollwertkombinationen, physikalische und biochemische Grenzen und der Einfluss der Prozessparameter werden untersucht. Mithilfe des Feedback linearisierten Modells werden zwei Regelstrategien, ein Feedforwardregler und ein Modell Prädiktiver Regler mit Zustandsbeobachtung, entworfen und analysiert. Es zeigt sich, dass durch die Verwendung von zwei unabhängigen Kohlenstoffquellen der Prozess dynamisch gesteuert werden kann. Durch die Wahl der Sollwerte kann das Verhältnis zwischen SSL und BALI™ beeinflusst werden. Insbesondere bei schwankenden Konzentrationen der Zuläufe zeigen die vorgeschlagenen Regelungsstrategien ihr Potenzial - durch entsprechende Anpassung der Prozessführung kann ein stabiler Zustand aufrechterhalten werden.

Contents

List of figures

List of tables

List of abbreviations, variables and parameters

Abbreviations

Abbreviation	Explanation
BALI™	spruce hydrolysate from Borregaard's advanced lignin process
C. glutamicum	*Corynebacteria glutamicum*
CER	carbon dioxide evolution rate
CPP	critical process parameters
CQA	critical quality attributes
CSTR	continuous stirred tank reactor
DO	dissolved oxygen
FF	feedforward control
G	glucose
HMF	hydroxy-methyl-furfural
HPLC	high pressure liquid chromatography
IPTG	Isopropyl-β-D-thiogalactopyranosid
LTI	linear time invariant
M	mannose
MIMO	multiple input multiple output
MPC	model predictive control
MPC1	model predictive control - strategy 1
MPC2	model predictive control - strategy 2
MPC3	model predictive control - strategy 3
OPC	open platform communication
OUR	oxygen uptake rate
PIMS	process information management system
SSL	spent sulfite liquor
T	nutrients

Abbreviation	Explanation
TR	temperature measurement and recording
TU Wien	Technische Universität Wien
WR	weight measurement and recording
X	biomass
XR	concentration measurement and recording

Biological variables

Variable	Explanation	Unit
c	mass concentration	g/L
c_i	mass concentration of component i in reactor	g/L
$c_{i,k}$	mass concentration of component i in in-/outlet k	g/L
CER	carbon dioxide evolution rate	mol/h
m	mass	g
m_i	mass of component i	g
$\dot{m}_{i,k}$	mass flow of component i in in-/outlet k	g/h
$\dot{m}_{i,R}$	production or consumption rate of component i	g/h
OUR	oxygen uptake rate	mol/h
q_i	biomass-specific glucose uptake rate of component i	g/gh
Q_i	volumetric reaction rate of component i	g/Lh
V	volume	L
V_R	liquid reactor volume	L
$\dot{V}_{air,in}$	volumetric air flow into the reactor	Nm^3/h
$\dot{V}_{air,out}$	volumetric air flow out of the reactor	Nm^3/h
$\dot{V}_B$	BALI™ feed rate	L/h
$\dot{V}_{BL}$	bleed rate	L/h
$\dot{V}_H$	harvest rate	L/h
$\dot{V}_N$	nutrient feed rate	L/h
$\dot{V}_S$	SSL feed rate	L/h
$y_{i,j}$	molecular concentration of component i in in-/outflow k	mol/Nm^3
μ	biomass-specific growth rate	1/h

Parameters of kinetic model

Parameter	Explanation	Value	Unit	Source
DoR_{O_2}	degree of reduction of oxygen	-4	mol_{e^-}/Cmol	[1]
DoR_s	degree of reduction of sugars	4	mol_{e^-}/Cmol	[1]
DoR_X	degree of reduction of biomass	4.18	mol_{e^-}/Cmol	[1]
$K_{S,G}$	glucose saturation constant	0.0948	g/L	[1]
$K_{S,M}$	mannose saturation constant	0.104	g/L	[1]
$M_{W,s}$	molecular mass of sugars	30.03	g/Cmol	[1]
$M_{W,X}$	molecular mass of biomass	27.78	g/Cmol	[1]
$q_{G,max}$	maximal biomass-specific glucose uptake rate	0.640	g/gh	[2]
$q_{M,max}$	maximal biomass-specific mannose uptake rate	0.0692	g/gh	[2]
$Y_{X/G}$	yield glucose to biomass	0.527	g/g	[2]
$Y_{X/M}$	yield mannose to biomass	0.377	g/g	[2]
$Y_{X/T}$	yield nutrients to biomass	0.0066	g/g	-

Variables in control theory

Variable	Explanation
$\boldsymbol{a}(\boldsymbol{x})$	vector field
$\boldsymbol{A}$, $\boldsymbol{A_d}$	system matrix of linearized system (continuous/discrete time)
$\tilde{\boldsymbol{A}}$	augmented system matrix of linearized system (discrete time)
$\boldsymbol{b}(\boldsymbol{x})$	system vector for maintainance
$\boldsymbol{B}$, $\boldsymbol{B_d}$	input matrix of linearized system (continuous/discrete time)
$\tilde{\boldsymbol{B}}$	augmented input matrix of linearized system (discrete time)
$\boldsymbol{C}$, $\boldsymbol{C_d}$	output matrix of linearized system (continuous/discrete time)
$\tilde{\boldsymbol{C}}$	augmented output matrix of linearized system (discrete time)
$\boldsymbol{D}(\boldsymbol{x})$	decoupling matrix
$\boldsymbol{e}$	control error
$\boldsymbol{f}(\boldsymbol{x})$	system function vector
$\boldsymbol{F}$	MPC system matrix
$\boldsymbol{g}(\boldsymbol{x})$, $\boldsymbol{g}_i(\boldsymbol{x})$	input function matrix / vector for input i
$\boldsymbol{h}(\boldsymbol{x})$	output function vector
$h_j(\boldsymbol{x})$	output function of output j

Variable	Explanation
J	cost function
k	time point in discrete time
$L_{\boldsymbol{a}}\lambda$	Lie-Derivative of $\lambda(\boldsymbol{x})$ along $\boldsymbol{a}(\boldsymbol{x})$
n_m, n_u, n_y	system/input/output order
N_c, N_p	control/prediction horizon
m	in-/output order
$\boldsymbol{Q}(\boldsymbol{x})$	observability matrix
$\boldsymbol{Q}_y$	weight matrix system outputs
$\boldsymbol{R}$	weight matrix system inputs
s	complex variable of the Laplace-transformation
$\boldsymbol{t}(\boldsymbol{x})$	diffeomorphism
T_s	sampling time
$\boldsymbol{u}$, $\boldsymbol{u_k}$	(discrete) input vector
$\boldsymbol{u}^{\min}$, $\boldsymbol{u}^{\max}$	maximal/minimal input vector
u_i	input i
$\boldsymbol{v}$, $\boldsymbol{v_k}$	(discrete) synthetic input vector
$\boldsymbol{v}^{\min}$, $\boldsymbol{v}^{\max}$	maximal/minimal synthetic input vector
v_i	synthetic input i
$V_i(\mathrm{s})$, $V_i(\mathrm{z})$	Laplace-/z-transformed synthetic input i
$\boldsymbol{x}$, $\hat{\boldsymbol{x}}$	(estimated) state vector
$\boldsymbol{y}$, $\hat{\boldsymbol{y}}$	(estimated) output vector
$\boldsymbol{y}(k+1\|k)^{\mathrm{T}}$	predicted output vector at $k+1$ with measurements until k
$\boldsymbol{y}^{\min}$, $\boldsymbol{y}^{\max}$	maximal/minimal output vector
y_j	output i
$\boldsymbol{y_{meas}}$, $\boldsymbol{y_{real}}$	measured/real output vector
$\boldsymbol{y}_*$, $\boldsymbol{Y}_*$	desired output trajectory vector/matrix
$\boldsymbol{Y}$	output matrix
$Y_i(\mathrm{s})$, $Y_i(\mathrm{z})$	Laplace-/z-transformed output i
z	complex variable of the z-transformation
$\boldsymbol{z}$, $\tilde{\boldsymbol{z}}$	(augmented) state vector of linearized system
z_i	state i of linearized system
δ, δ_i	relative degree (of output i)
$\boldsymbol{\Delta u}^{\min}$, $\boldsymbol{\Delta u}^{\max}$	maximal/minimal change of input vector
$\boldsymbol{\Delta v}^{\min}$, $\boldsymbol{\Delta v}^{\max}$	maximal/minimal change of synthetic input vector
$\boldsymbol{\Delta V}$	synthetic input matrix
$\lambda(\boldsymbol{x})$	scalar function
$\xi_{i,j}$, $\eta_{\delta+i}$	external/internal state
$\boldsymbol{\Phi}$	MPC input matrix

Chapter 1

Introduction

The manufacturing of products through biotechnological processes is indispensable nowadays. [3] Microorganisms are widely used in the pharmaceutical industry for the production of vaccines, hormones, antibiotics and antibodies, in the energy sector for the production of bio-fuel and renewable energy, in sewage plants and in the food, chemical and agricultural industry [4]. Often, biotechnological processes are a more cost-, energy- and resource-efficient alternative to chemical synthesis or physical processes. Furthermore, a variety of products is not producible by humans without the cultivation of microorganisms [3].

However, the carbon sources required for many biotechnological processes are widely obtained from high-value sugar- and starch-containing plant material, which is also used in the production of food [5]. Therefore, there is a high demand in alternative carbon-sources, which are mainly sought in the waste products of other processes [6]. The usage of secondary raw materials is of great interest, because the recycling of waste products could lead to more cost-efficient and ecological processes with products that have improved live cycles making their contribution to an overall circular economy [5]. Nevertheless, due to the complex composition of the waste streams as well as possible inhibitory components a good understanding of their effects on the microorganism and production process is inevitable [2].

Current research focuses on lignocellulosic waste streams from the paper and pulping industry due to their high total sugar concentrations [7] as well as their large annual production volumes [8]. Around sixty percent of the world's paper and pulp demand is produced in the sulfite process with the waste stream *spent sulfite liquor* (SSL) [8], leading to an annual production of around ninety billion liters [9]. Although used in the production of some high-value products, such as Xylitol, Xylanase and Vanillin as well as low-value Ethanol [8], around three-quarters of SSL are incinerated [10].

Finding further applications for the production of high-value products is therefore highly desirable [7]. However, bioprocessing with SSL is challenging due to its complex composition [11], including various sugar compounds, such as arabinose, glucose, galactose, mannose and xylose, and potentially growth-inhibiting compounds, such as sulfite, furfural and hydroxy-methyl-furfural (HMF) [2].

To achieve good efficiency of the promising high total sugar amount, it is necessary to process with microorganisms that can efficiently metabolize several of the sugar components [7]. Due to its ability to consume different sugars available in the SSL [12] as well as its high tolerance for organic acids such as acetate [5], the soil bacteria *Corynebacteria glutamicum* has shown promising results when processed with SSL [1, 2, 11]. Several production routs of *C. glutamicum* have been established for the production of more than seventy high-value compounds [12], making *C. glutamicum* an important expression host in biotechnology [5].

However, for effective and economically favourable production with SSL as a complex substrate and *C. glutamicum* as host organism, composition and possible inhibitory effects of SSL on the production process must be identified and analysed [2]. By using model-based approaches for systematic and target-oriented process development, the influence of critical process parameters (CPP) on critical quality attributes (CQA) can be identified [13]. Additionally, a better process understanding can be obtained which provides a sound basis for the design of a complex control strategy and consequently the development of cost-efficient, optimized and ecological processes [14].

Using secondary raw materials as cultivation media, the composition of the complex media is predetermined by the preceding process and its raw materials [8]. Varying concentrations of sugars in the SSL can be dynamically compensated by adding other carbon sources. Spruce hydrolysate from Borregaards advanced lignin process (BALI™) is such a suitable alternative with high glucose concentrations [10]. In addition, undesirable interactions between the medium and needed nutrients or low solubility of nutrients in the medium can occur. A separate addition of these nutrients can be a possibility to ensure stable and productive processes [15]. Multiple feeds are therefore needed to control such a process in a sufficient way, leading to a complex, nonlinear *multiple input multiple output* control problem.

The optimal control to obtain and maintain beneficial growth conditions is of high importance. Productivity loss and cell death due to under-feeding or extensive by-product formation as well as nutrient and inhibitor accumulation due to over-feeding can be avoided by accurate process development [16]. Nowadays, bioprocesses are controlled with both conventional control strategies in open and closed loop and modern control strategies, such as neural network-based control, fuzzy logic, adap-

tive control and model predictive control (MPC) [14]. However, the processes within the bioreactor are complex and nonlinear [17]. Conventional control strategies are not able to account for these nonlinearities [14]. Nevertheless, in industry, simple feedforward control with constant feed rates [13] as well as conventional control strategies [17] are still commonly used. Consequently the development, implementation and realisation of advanced control strategies are necessary to ensure stable, productive and beneficial processes [16]. Furthermore, due to relatively large time constants of the processes, the implemented control strategies may be computationally intensive, enabling the usage of advanced and complex nonlinear control strategies.

Nonlinear feedback linearization has been studied for the control of bioprocesses for simple process models with promising results [16, 17, 18, 19, 20, 21, 22, 23]. A linear and decoupled system is obtained from the nonlinear model by an invertible nonlinear coordinate transformation [20]. Well-known linear methods can be applied to the linear model [24] and by transforming the system back, a nonlinear control law is obtained that compensates all nonlinearities of the model [25]. Combining the advantages of linear and nonlinear control methods, feedback linearization enables robust and accurate control [25].

When designing a process controller for a bioprocess, ecological aspects must be part of the strategy. The choice of setpoints or trajectories, process parameters and input levels should be optimized in order to lead to a resource- and energy-efficient process while minimizing by- and waste product formation [14]. Minimal usage of feedstocks and sufficiently low sugar concentrations at the end of continuous bioprocesses are aspects that have to be considered when implementing control strategies [16].

Furthermore, the availability of data and real-time measurements during bioprocesses is a big challenge. Some biological key variables can be obtained only by offline, cost- and time-intensive measurements [14]. For example, sugar concentrations in the broth are usually measured by high pressure liquid chromatography (HPLC) and are therefore not available in real-time. To address this problem, state observers can be implemented - using online measurements in combination with the process model, states, that are not or hard to measure with sufficient sampling time, can be estimated. Therefore, the total cost for measuring can be reduced while simultaneously improving the process observation [16]. During fermentation, offgas measurements are usually available in real time and can be used to calculate the amount of oxygen consumed and the carbon dioxide produced, known as the oxygen uptake rate OUR and carbon dioxide evolution rate CER, which are proven to reflect the processes taking place inside the reactor [11].

In this thesis, a control strategy for a given process is designed and experimentally validated. *C. glutamicum* is fermented in a continuous stirred tank reactor (CSTR) and fed with the waste streams SSL and BALI™ from the pulping industry and a solution providing nutrients. After the fermentation reactor, a membrane module is installed for cell retention, enabling an increase of biomass concentration in the reactor and continuous harvesting. By controlling the three feeds, the harvest and the bleed rate the objective of a beneficial and stable process is achieved. Based on a nonlinear process model derived from literature [1, 2] with state coupling, a nonlinear control law is found by the method of feedback linearization for the *multiple input multiple output* (MIMO) system, enabling a model-based control strategy, that incorporates the non-linearities of the identified model. The feedback linearized model is used to design a feedforward controller and an MPC with state estimation to handle the poor measureability of sugar and biomass concentration.

Furthermore, a feasibility analysis of various setpoints is made with the feedback linearized system in order to identify beneficial process settings. The process and the control strategies are examined for stability when parameter deviations occur. Consequently, the possible influence of certain uncertainties and model-plant mismatches on the process are examined. Different possible measurement scenarios for the MPC are compared. The results from experimental runs at laboratory scale are analysed to show the the quality and potential of the proposed control strategy.

The thesis is structured as follows. In chapter 2 the cultivation process is described, the bacteria and used materials are defined and the environmental beneficial aspects are discussed. Additionally, the experimental setup is described. The nonlinear process model is identified and parametrized in chapter 3. In chapter 4 the necessary theory for the development of the control strategy is given, namely the method of feedback linearization, the basics of feedforward control and the principle of model predictive control with state estimation. The theory is then applied in chapter 5 to the previous established model. Beneficial setpoint combinations are identified, the system behaviour for varying parameters is examined and different measurement scenarios for the MPC are studied in chapter 6. The results of the experiments carried out in the laboratory reactor with the introduced control strategy are presented in chapter 7. In chapter 8 the outcomes of the work are summarized, analyzed and discussed. Finally, a short conclusion is given in chapter 9 along with an outlook on the further potential of the applied method.

Chapter 2

Fermentation process and experimental setup

Wild type *C. glutamicum* ATCC13032 is fermented with two lignocellulosic waste waters from the pulp industry in a continuous fermentation process with cell retention. Due to its ability to grow on different carbon sources and its high tolerance for organic acids such as acetate, *C. glutamicum* is a good candidate for bioprocessing on raw materials containing non-native carbon sources [12]. With over seventy different products such as *L-Lysine*, *L-Glutamate* and *L-Valine* [2], *C. glutamicum* has become one of the workhorses of white biotechnology [2]. In addition, it is an extensively studied organism with a variety of genetically engineered strains for better media usage [12]. The soil bacteria has shown its potential when fermented with SSL in recent studies [1, 2, 11]. During the continuous process, *mCherry* production induced by IPTG is analysed. *mCherry* is a red fluorescence protein, which can be detected clearly by fluorescence spectroscopy due to its unique color [26].

Lignocellulosic waste products from the pulp industry are promising alternative carbon sources for bioprocessing [7] due to the high sugar concentrations [8]. Recycling these waste streams, which are currently mostly combusted [10], allows low-value materials to be turned into high-value products [6] and helps to create a circular economy by reducing pollution [7]. However, different raw materials and conditions of the pulp production result in varying compositions in the waste waters making the valorization of SSL challenging [8]. By using an additional carbon source concentration deviations in the SSL can be compensated and the problem of raw material uncertainty can be tackled. SSL, with an annual production of over ninety billion liters [9], is used as the main carbon source. By adding small amounts of the higher valued BALI™ to the broth, the process is controlled so that a stable and beneficial

state is maintained. The recycling of SSL and BALI™ can be done efficiently while reducing the composition requirements. Furthermore, low solubility of nutrients in the SSL and BALI™ can be counteracted by adding an additional feed containing these limiting components.

The fermentation is carried out in a continuously stirred tank reactor (CSTR) with a working volume of 7.5L (Labfors 5, Infors HT, Bottmingen, Switzerland) with baffles at the facilities of *TU Wien - Institute of Chemical, Environmental and Bioscience Engineering*. The broth is mixed with a disk impeller stirrer (800 to 1200 rpm). Clean compressed air is added to the reactor with a gasing rate of 0.5vvm. The SSL is mixed with supplemental glucose and mannose to achieve a concentration profile during the fermentation in the SSL tank with a working volume of 3.6L (Labfors 5, Infors HT, Bottmingen, Switzerland). The SSL tank, BALI™, nutrition feed as well as acid and base for pH control are connected to the reactor. Two hollow fiber microfiltration modules (Microza PSP-113, Asahi Kasei, Chiyoda, Japan), with a polyolefin membrane, a pore size of 0.1 µm, a fiber diameter of 1.9 mm and a membrane area of 0.1 m^2, for cell retention are connected to the reactor and operated with a loop pump (V6-3L, SHENCHEN, Baoding, China) at 1.5 L/min. The permeate side of the membrane modules are connected with the harvest tank. Furthermore, the bleed tank is connected to the reactor. Samples for offline analysis are taken from the reactor using an automated sampling system (custom made by the Institute of Chemical, Environmental and Bioscience Engineering, TU Wien, Vienna, Austria) every three hours and at refill from SSL tank. The samples are stored at 4°C using a fraction collector (FC 203B, Gilson, Middleton, USA) for later analysis. The process flow chart of the system is displayed in Figure 2.1.

The temperature was kept at 30°C. The culture pH was hold constant at 7 by adding 2.5 M KOH and 2.5 M H_2SO_4 accordingly. The used SSL with 44 g/L glucose and 138 g/L mannose and BALI™ with 504 g/L glucose and 26 g/L mannose are diluted to 25% of their undiluted concentration. Varying concentrations of the SSL were achieved by adding glucose and mannose. All media were supplemented with antibiotics (50 µg/mL kanamycin sulfate). The ultra-filtered SSL, autoclaved BALI™ and ultra-filtered nutrient solution containing urea as nitrogen source and KH_2PO_4 as phosphorous source are added with the calculated feed rates. The process is inoculated with a preculture so that an initial optical density at 600 nm of one is obtained. After 100h, *mCherry* production is induced with IPTG.

The online measurements are taken continuously and stored in the process information management system (Lucullus, Securecell, Urdorf, Switzerland). The offgas analyzer (Blue in One, Blue Sence, Heidelberg, Germany) measures the O_2 content

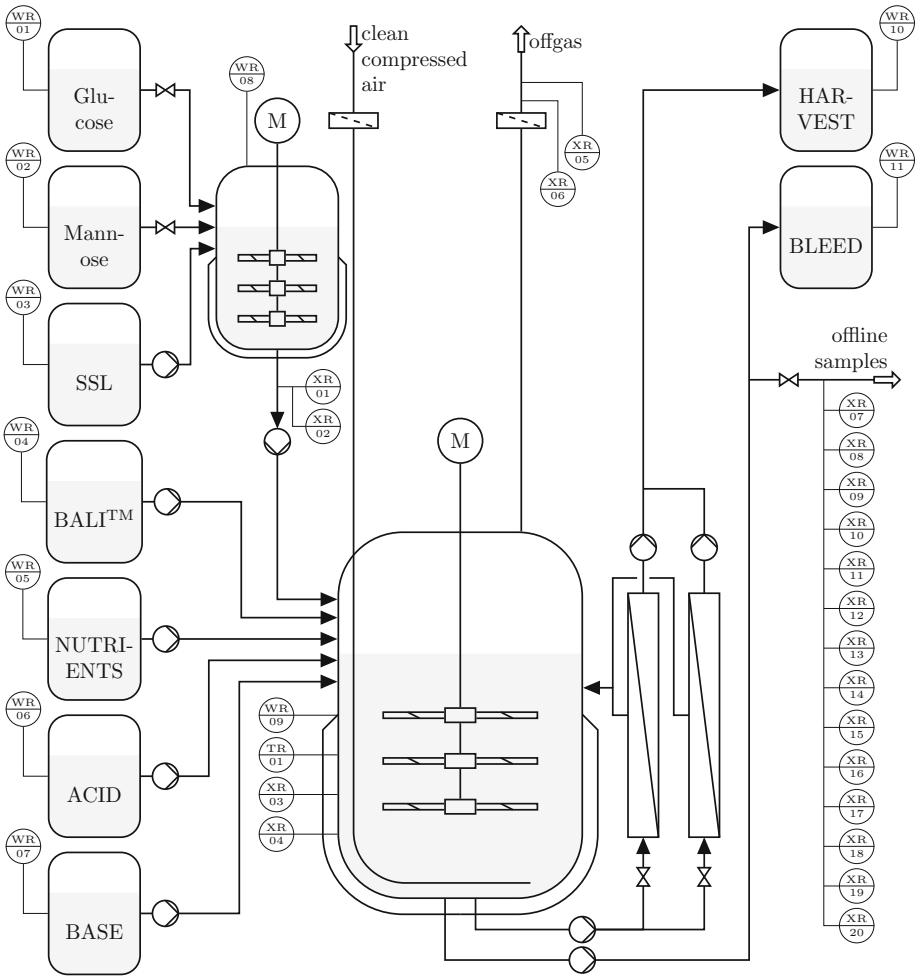

Figure 2.1: Flow chart of experimental setup. The equipment used and the measurements made during the process are represented. Glucose, mannose and SSL are premixed in the SSL tank. BALI™, nutrients, acid and base are connected directly to the fermentation reactor. The membrane modules for cell retention are attached to the harvest tank on the permeate side. Points of weight (WR), concentration (XR) and temperature (TR) measurements are labeled (see also Table 2.1).

(XR06) based on galvanic cells and the CO_2 content (XR05) with infrared sensor modules continuously. The weights of the reactor and storage tanks (Glucose, Mannose, SSL, BALI™, nutrients, acid, base, SSL tank, fermentation reactor, harvest, bleed (WR01-11)) are measured continuously for the calculation of the reactor volume and volumetric rates. Temperature (TR01), pH (XR04) and pO_2 (XR03) are mea-

sured inline with a thermometer, pH electrode (Hamilton, Bonaduz, Switzerland) and DO electrode (Hamilton, Bonaduz, Switzerland) respectively. The online signals are transferred via the open platform communication server (OPC server) from the process information management system (PIMS) to MATLAB 2020a (MATALB 2020a, MathWorks, Natick, USA) for online data processing. The processed data and calculated signals, such as the feedrates, are send back to the PIMS, which can then adjust the physical properties of the process equipment accordingly. The main components of the experimental setup are displayed in Figure 2.2.

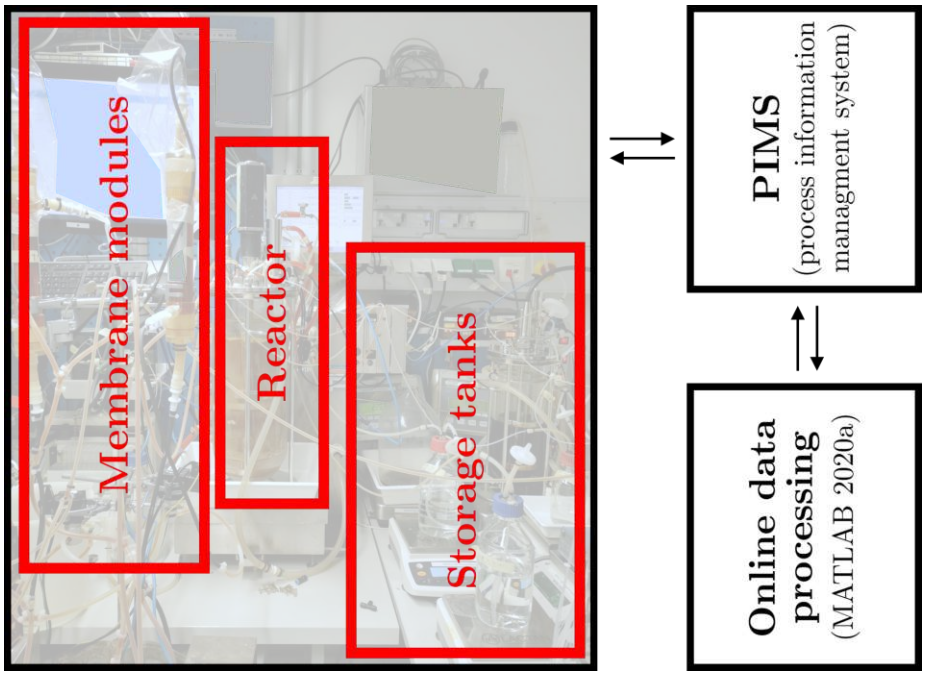

Figure 2.2: Flow of information between components of the experimental setup. The results from the online measurements are stored in the process information management system (PIMS) and send to MATLAB 2020a for online data processing via an open platform communication (OPC) server. The online signals are processed and the resulting signals are written to the PIMS which can then communicate to corresponding reactor equipment to obtain the desired process behavior.

From the offline samples, biomass was measured gravimetrically (XR07) as dry cell weight by centrifuging 1.8 ml broth (14000 g, 4°C, 10 min) and drying the resulting pellet in an oven (95°C, 72 h). Concentrations of sugars, namely glucose, mannose, xylose and arabinose (XR08-11), urea (XR12) and inhibitory compounds furfural (XR13) and HMF (XR14) were measured form the resulting supernatant by

HPLC (UltiMate 3000, thermo fischer scientific, Waltham, USA) with a isocratic flow of 0.4 ml/min of ultra pure water on a lead column (NUCLEOGEL SUGAR Pb 719530, Macherey-Nagel, Düren, Germany) using a RI-Detector (Shodex RI-101, Showa Denko, Tokio, Japan). Furthermore the glucose (XR01) and mannose (XR02) concentrations in the SSL were measured with the same HPLC procedure. Using an enzyme assay pipetting robot (Cedex BioHT, Roche, Basel, Switzerland), the concentration of organic acids acetate, lactate and glutamate (XR15-17) as well as the concentration of nutrients ammonia and phosphate (XR18-19) were measured from the supernatant. For the measurement of *mCherry* (XR20), the earlier described cell pellets were resuspended in 0.9% NaCl and fluorescence was measured (TECAN SPARK, Tecan, Männedorf, Switzerland) with an excitation at 560 nm and an emission at 610 nm. The measurements conducted during the process are listed in Table 2.1.

Table 2.1: Online and offline measurements during process. The temperature (TR), weight (WR) and concentration (XR) measurements conducted during the process are listed.

Code	Measurement	Code	Measurement
TR01	temperature reactor	XR05	CO2 offgas
WR01	weight glucose	XR06	O2 offgas
WR02	weight mannose	XR07	biomass concentration
WR03	weight SSL	XR08	glucose concentration
WR04	weight BALI™	XR09	mannose concentration
WR05	weight nutrients	XR10	xylose concentration
WR06	weight acid	XR11	arabinose concentration
WR07	weight base	XR12	urea concentration
WR08	weight SSL tank	XR13	furfural concentration
WR09	weight fermentation reactor	XR14	HMF concentration
WR10	weight harvest	XR15	acetate concentration
WR11	weight bleed	XR16	lactate concentration
XR01	glucose concentration SSL	XR17	glutamate concentration
XR02	mannose concentration SSL	XR18	ammonia concentration
XR03	pO2 broth	XR19	phosphate concentration
XR04	pH broth	XR20	mCherry concentration

Chapter 3

Modelling and parameterization

For better process understanding and the ability to implement an advanced model-based control strategy, a mathematical model of the process is identified and parameterized. In order to describe the biochemical reactions, the kinetic model and the corresponding parameters (section 3.1), which mathematically describe the reaction rates, are based on published models and parameters, which are obtained from experiments with the same bacterial strain and SSL as carbon source [1, 2]. Inhibitory glucose and mannose consumption is modelled. The model is extended to include nutrient demand. Additionally, the differential equations are derived from the mass balances around the reactor (section 3.2).

3.1 Kinetic model

The biomass in the reactor consumes substrate, grows and produces protein and byproducts. In order to describe the processes within the system, an unstructured kinetic model is established. Unstructured models, which are characterized by a macroscopic approach [3], consider the mass concentration of the biomass as only biological state variable [16]. Processes within the cells, the molecular composition of the cell and the size and age of the organisms are considered to be homogeneous in all cells [27]. Using these assumptions, simple but accurate models can be established that are widely used in both industry [19] and research [20].

The sugars glucose and mannose are fed to the biomass and burned aerobically. Furthermore, nutrients are needed for biomass growth and protein production. The consumption of sugar as carbon source, oxygen O_2 and nutrients T leads to the

production of biomass X and CO_2. This processes can be summarized with the reaction equation

$$\text{Sugar} + O_2 + T \xrightarrow{X} X + CO_2.$$

Glucose uptake. The biomass-specific glucose uptake is described by the Monod kinetic

$$q_G = q_{G,max} \frac{c_G}{c_G + K_{S,G}} \tag{3.1}$$

where q_G is the biomass specific glucose uptake rate in g/gh, $q_{G,max}$ is the maximum biomass specific glucose uptake rate in g/gh, c_G is the glucose concentration in g/L and $K_{S,G}$ is the glucose saturation constant in g/L. The course of q_G as function of the glucose concentration is displayed in Figure 3.1. **Mannose uptake.** The

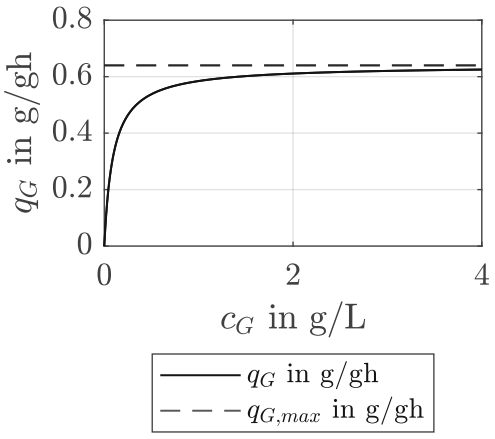

Figure 3.1: Biomass specific glucose uptake. The biomass specific glucose uptake is described by a Monod kinetic. High glucose concentration lead to high substrate uptake ($c_G >> K_{S,G} \rightarrow q_G \approx q_{G,max}$). However, Controllability over the system is only given at low glucose concentrations ($q_G << q_{G,max}$).

mannose uptake is modelled with the Monod kinetic including an inhibitory effect of the glucose concentration on the mannose uptake

$$q_M = q_{M,max} \frac{c_M}{c_M + \frac{K_{S,M}}{K_{S,G}} c_G + K_{S,M}} \tag{3.2}$$

where q_M is the biomass specific mannose uptake rate in g/gh, $q_{M,max}$ is the maximum biomass specific mannose uptake rate in g/gh, c_G is the glucose concentration in g/L, c_M is the mannose concentration in g/L, $K_{S,G}$ is the glucose saturation constant in

g/L and $K_{S,M}$ is the mannose saturation constant in g/L. The course of q_M as function of the glucose and mannose concentration is displayed in Figure 3.2. It can be seen, that small changes at low glucose concentrations do influence the mannose uptake significantly.

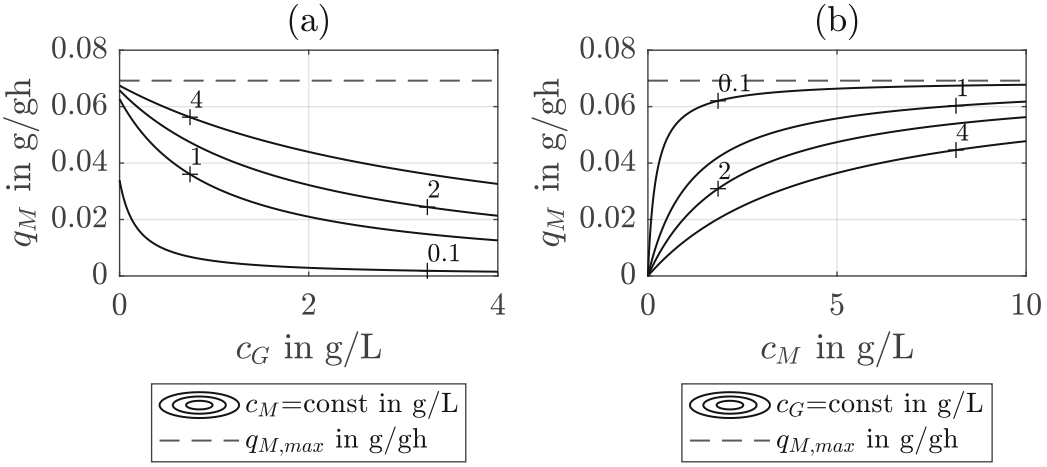

Figure 3.2: Biomass specific mannose uptake. (a) Due to the inhibitory effects of the glucose concentration on the mannose uptake, the biomass specific mannose uptake decreases quickly with increasing glucose concentrations. (b) For constant glucose concentrations, the mannose uptake follows Monod kinetic. The biomass specific mannose uptake and consumption can consequently be controlled by varying the glucose and mannose concentrations.

Biomass growth. The specific biomass growth rate is described by the biomass specific sugar uptake rates and the constant yields

$$\mu = Y_{X/G} q_G + Y_{X/M} q_M \tag{3.3}$$

where μ is the biomass specific growth rate in 1/h, q_G is the biomass specific glucose uptake rate in g/gh, q_M is the biomass specific mannose uptake rate in g/gh, $Y_{X/G}$ is the constant yield from glucose to biomass in g/g and $Y_{X/G}$ is the constant yield from mannose to biomass in g/g. The course of μ as function of the glucose and mannose concentration is displayed in Figure 3.3.

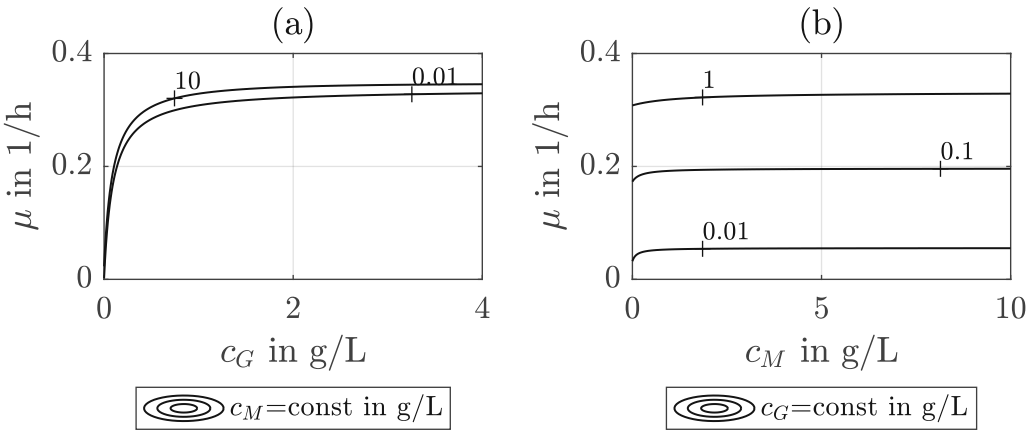

Figure 3.3: Specific biomass growth. (a) The lines for c_M = const are almost on top of each other, despite the large differences ($c_M = \{0.01, 10\}$ g/L). (b) This effect becomes also visible by the almost parallel lines for c_G = const. Consequently, biomass growth strongly depends on the glucose concentration.

Nitrogen and phosphor demand. The nitrogen and phosphor demand for biomass growth is proportional to the biomass specific growth μ and is therefore described by

$$q_T = \frac{\mu}{Y_{X/T}} \tag{3.4}$$

with the biomass specific nitrogen and phosphor demand q_T in g/gh and the constant demand of nutrients for biomass growth $Y_{X/T}$. Consequently, the biomass specific nutrient demand correlates directly with μ.

Oxygen uptake and carbon dioxide formation. The oxygen uptake rate

$$\text{OUR} = \frac{c_X V_R}{DoR_{O_2}} \left(DoR_s \frac{q_G + q_M}{M_{W,s}} - DoR_X \frac{\mu}{M_{W,X}} \right) \tag{3.5}$$

and carbon dioxide formation rate

$$\text{CER} = c_X V_R \left(\frac{q_G + q_M}{M_{W,s}} - \frac{\mu}{M_{W,X}} \right) \tag{3.6}$$

are modelled as function of the reactor volume V_R in L, the biomass concentration c_X in g/L and the biomass specific rates (q_S, q_M, μ). Furthermore the molecular weights of the sugars $M_{W,s}$ and the biomass $M_{W,X}$ in g/Cmol and the Degree of Reduction of oxygen DoR_{O_2}, sugar DoR_s and biomass DoR_X in mol_{e^-}/Cmol are needed. [1]

3.2 Mass balance and differential equations

The system differnetial equations are derived from the mass balance around the reactor. In Figure 3.4 the in- and outflows of the reactor and modelled states are displayed.

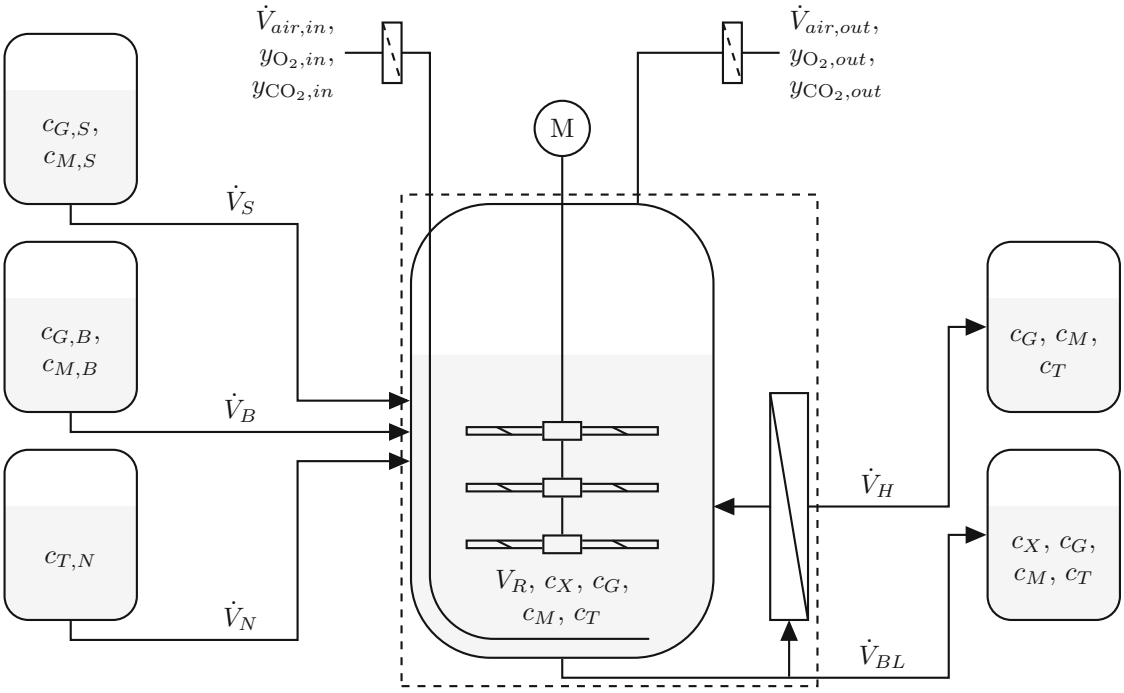

Figure 3.4: Schematic model of bioreactor with cell retention. The scheme of the continuous stirred tank reactor is displayed with all the modelled inputs, outputs and states. The system boundaries (dashed line) for the mass balance are displayed. By adapting the SSL feed $\dot{V}_S$ with the glucose $c_{G,S}$ and mannose concentration $c_{M,S}$, the BALI™ feed $\dot{V}_B$ with the glucose $c_{G,B}$ and mannose concentration $c_{M,B}$, the nutrient feed $\dot{V}_N$ with the nutrient concentration $c_{T,N}$, the harvest rate $\dot{V}_H$ and the bleed rate $\dot{V}_{BL}$ the states in the reactor, namely the reactor volume V_R, the biomass c_X, glucose c_G, mannose c_M and nutrient concentration c_T can be influenced. Furthermore the airflow in $\dot{V}_{air,in}$ and out $\dot{V}_{air,out}$ of the reactor with the corresponding oxygen and carbon dioxide molar concentrations ($y_{O_2,in}$, $y_{CO_2,in}$, $y_{O_2,out}$, $y_{CO_2,out}$) is monitored.

The liquid feeds SSL ($\dot{V}_S$ in L/h), BALI™ ($\dot{V}_B$ in L/h) and nutrients ($\dot{V}_N$ in L/h), the harvest ($\dot{V}_H$ in L/h) and bleed rate ($\dot{V}_{BL}$ in L/h) as well as the airflow in ($\dot{V}_{air,in}$

in Nm^3/h) and out ($\dot{V}_{air,out}$ in Nm^3/h) of the reactor are considered. The following model assumptions and simplifications are made

Ideally stirred tank reactor. The reactor is assumed to be an ideally stirred tank reactor. Therefore the mass concentrations are independent of the position in the reactor ($dc_i/dx = 0$).

Cell Retention. The membrane module for the cell retention holds back the biomass and lets all other components of the broth pass. The sugar and nutrient concentrations in the harvest are therefore equal to the concentrations within the reactor.

Inlets and Outlets. All mass-flows in and out of the reactor are described by the modelled in- and outlets ($\dot{V}_S$, $\dot{V}_B$, $\dot{V}_N$, $\dot{V}_H$, $\dot{V}_{BL}$, $\dot{V}_{air,in}$, $\dot{V}_{air,out}$). O_2 and CO_2 are the only volatile components of the modelled system. The balance around the liquid reactor volume becomes

$$\frac{dV_R}{dt} = \dot{V}_S + \dot{V}_B + \dot{V}_N - \dot{V}_H - \dot{V}_{BL}. \tag{3.7}$$

Concentrations in Inlets and Outlets. In Table 3.1 the mass and molecular concentrations in the feeds, outlets and air flow are displayed.

Table 3.1: Concentrations of components in in- and outlets: The mass $c_{i,k}$ in g/L and molecular concentrations $y_{i,k}$ in mol/Nm^3 of the components i in the in- and outlets k are listed. No occurrence of the component in the corresponding flow is displayed as empty cell ($c_{i,k} = 0$ g/L or respectively $y_{i,k} = 0$ mol/Nm^3).

	Feeds			Outlets		air flow	
	S	B	N	H	BL	in	out
Biomass X					c_X		
Glucose G	$c_{G,S}$	$c_{G,B}$		c_G	c_G		
Mannose M	$c_{M,S}$	$c_{M,B}$		c_M	c_M		
Nutrients T			$c_{T,N}$	c_T	c_T		
Oxygen O_2						$y_{O_2,in}$	$y_{O_2,out}$
Carbon dioxide CO_2						$y_{CO_2,in}$	$y_{CO_2,out}$

The **mass balance for a single compound i of the liquid phase** is

$$\frac{dm_i}{dt} = \dot{m}_{i,R} + \sum_{k=\{S,B,N\}} \dot{m}_{i,k} - \sum_{k=\{H,BL\}} \dot{m}_{i,k} \tag{3.8}$$

with the absolute rate of mass change dm_i/dt in g/h, the production or consumption rate $\dot{m}_{i,R}$ in g/h and the mass flows in and out of the reactor $\dot{m}_{i,k}$ in g/h of component i. With $m = cV$, partial deviation and Equation 3.7 the concentration balance for an ideally stirred tank reactor and one component i

$$\frac{dc_i}{dt} = Q_i + \sum_{k=\{S,B,N\}} \frac{\dot{V}_k}{V_R}(c_{i,k} - c_i) - \sum_{k=\{H,BL\}} \frac{\dot{V}_k}{V_R}(c_{i,k} - c_i) \tag{3.9}$$

with the volumetric reaction rate $Q_i = \dot{m}_{i,R}/V_R$ can be formulated. With the concentrations in Table 3.1, $Q_i = q_i c_X$, the concentration balances for X, G, M and T as well as Equation 3.7, the needed differential equations

$$\frac{dV_R}{dt} = \dot{V}_S + \dot{V}_B + \dot{V}_N - \dot{V}_H - \dot{V}_{BL} \tag{3.10a}$$

$$\frac{dc_X}{dt} = \mu c_X - c_X \frac{\dot{V}_S + \dot{V}_B + \dot{V}_N - \dot{V}_H}{V_R} \tag{3.10b}$$

$$\frac{dc_G}{dt} = -q_G c_X - c_G \frac{\dot{V}_S + \dot{V}_B + \dot{V}_N}{V_R} + c_{G,S}\frac{\dot{V}_S}{V_R} + c_{G,B}\frac{\dot{V}_B}{V_R} \tag{3.10c}$$

$$\frac{dc_M}{dt} = -q_M c_X - c_M \frac{\dot{V}_S + \dot{V}_B + \dot{V}_N}{V_R} + c_{M,S}\frac{\dot{V}_S}{V_R} + c_{M,B}\frac{\dot{V}_B}{V_R} \tag{3.10d}$$

$$\frac{dc_T}{dt} = -q_T c_X - c_T \frac{\dot{V}_S + \dot{V}_B + \dot{V}_N}{V_R} + c_{T,N}\frac{\dot{V}_N}{V_R} \tag{3.10e}$$

$$\tag{3.10f}$$

for the reactor volume V_R, the biomass X, glucose G, mannose M, and nutrients T are obtained.

The oxygen uptake rate OUR and carbon dioxide evolution rate CER can be calculated with the **molecular balance for the volatile components** and the assumption $dy_i/dt = 0$, leading to

$$\mathrm{OUR} = \dot{V}_{air,out} y_{\mathrm{O_2},out} - \dot{V}_{air,in} y_{\mathrm{O_2},in} \tag{3.11a}$$

$$\mathrm{CER} = \dot{V}_{air,out} y_{\mathrm{CO_2},out} - \dot{V}_{air,in} y_{\mathrm{CO_2},in} \tag{3.11b}$$

with the volumetric air flow in $\dot{V}_{air,in}$ and out of the reactor $\dot{V}_{air,out}$ in $\mathrm{Nm^3/h}$ and the molecular concentrations in the inflow $y_{i,in}$ and outflow $y_{i,out}$ for the components oxygen and carbon dioxide in $\mathrm{mol/Nm^3}$ [28].

3.3 Parameterization

The model parameters and structure for biomass growth on glucose and mannose, namely for q_G, q_M and μ are derived from [2], where the parameters are fitted on data obtained from experiments with the same *C. glutamicum* strain processed with full defined media with SSL as sole carbon source. The parameters for the OUR and CER are derived from [1]. The parameters for nutrient demand are based on complementary experiments ensuring sufficient nutrient concentration and preventing precipitation due to low solubility. All numeric values for the parameters as well as the corresponding literature are listed in the List of Abbreviations, Variables and Parameters.

Chapter 4

Control theory

In the following chapter, the used methodology for the establishment of the control strategies is given. The method of feedback linearization (section 4.1), that transforms the nonlinear system into a linear system via an invertible nonlinear coordinate transformation, the fundamentals of feedforward control (section 4.2) and the principle of model predictive control (MPC) with state estimation (section 4.3) are defined.

4.1 Feedback linearization of MIMO systems

By the method of feedback linearization a nonlinear system can be transformed into a linear system with a nonlinear coordinate transformation. Then, a linear controller can be designed using well established linear control methods. By transforming the system back to the original coordinates, a nonlinear control law is obtained that incooperates all non-linearities of the system. The described method is therefore fundamentally different from Jacobian linearization that approximates the nonlinear behaviour around a point of operation [24]. The necessary definitions and equations of the method are given, the full method including mathematical proof can be found in [25].

The *input affine* system

$$\begin{aligned} \dot{\boldsymbol{x}} &= \boldsymbol{f}(\boldsymbol{x}) + \boldsymbol{g}(\boldsymbol{x})\boldsymbol{u} \\ \boldsymbol{y} &= \boldsymbol{h}(\boldsymbol{x}) \end{aligned} \tag{4.1}$$

with the state vector $\boldsymbol{x} \in \mathbb{R}^{n_m}$ of system order n_m, the time derivative of the state vector $\dot{\boldsymbol{x}} = d\boldsymbol{x}/dt$, the system function vector $\boldsymbol{f}(\boldsymbol{x}) \in \mathbb{R}^{n_m \times 1}$, the input function vector $\boldsymbol{g}(\boldsymbol{x}) = [\boldsymbol{g_1}(\boldsymbol{x}), \ldots, \boldsymbol{g_{n_u}}(\boldsymbol{x})] \in \mathbb{R}^{n_m \times n_u}$ for the n_u inputs $\boldsymbol{u} = [u_1, \ldots, u_{n_u}]^{\mathrm{T}} \in$

$\mathbb{R}^{n_u \times 1}$, the output function vector $\boldsymbol{h}(\boldsymbol{x}) = [h_1(\boldsymbol{x}), \ldots, h_{n_y}(\boldsymbol{x})]^{\mathrm{T}} \in \mathbb{R}^{n_y \times 1}$ for the n_y system outputs $\boldsymbol{y} \in \mathbb{R}^{n_y}$, that is linear in all inputs can be linearized by the nonlinear coordinate transformation. For the following considerations, the correlation $m = n_u = n_y$ is valid.

By defining the **Lie-Derivative**

$$L_{\boldsymbol{a}}\lambda = \frac{\partial \lambda(\boldsymbol{x})}{\partial \boldsymbol{x}} \boldsymbol{a}(\boldsymbol{x}) = \mathrm{grad}^T \lambda(\boldsymbol{x}) \boldsymbol{a}(\boldsymbol{x}). \tag{4.2}$$

of a scalar function $\lambda(\boldsymbol{x})$ along a vector field $\boldsymbol{a}(\boldsymbol{x})$, the time derivative of a single output $y_j = h_j(\boldsymbol{x})$

$$\begin{aligned} \dot{y}_j &= \frac{dh_j(\boldsymbol{x})}{dt} = \frac{\partial h_j(\boldsymbol{x})}{\partial \boldsymbol{x}} \frac{\partial \boldsymbol{x}}{dt} = \frac{\partial h_j(\boldsymbol{x})}{\partial \boldsymbol{x}} \dot{\boldsymbol{x}} \\ &= \frac{\partial h_j(\boldsymbol{x})}{\partial \boldsymbol{x}} \boldsymbol{f}(\boldsymbol{x}) + \frac{\partial h_j(\boldsymbol{x})}{\partial \boldsymbol{x}} \boldsymbol{g}_1(\boldsymbol{x}) u_1 + \cdots + \frac{\partial h_j(\boldsymbol{x})}{\partial \boldsymbol{x}} \boldsymbol{g}_m(\boldsymbol{x}) u_m \\ &= L_{\boldsymbol{f}} h_j(\boldsymbol{x}) + L_{\boldsymbol{g_1}} h_j(\boldsymbol{x}) u_1 + \cdots + L_{\boldsymbol{g_m}} h_j(\boldsymbol{x}) u_m \end{aligned} \tag{4.3}$$

can be obtained. The *input affine* system (Equation 4.1) has the **vector relative degree** $\{\delta_1, \delta_2, \ldots, \delta_m\}$ with the relative degree $\delta = \sum_{i=1}^{m} \delta_i \leq n$ if

(A) $L_{\boldsymbol{g}_j} L_{\boldsymbol{f}}^k h_i(\boldsymbol{x}) = 0$, $j = 1, \ldots, m$, $i = 1, \ldots, m$, $k = 0, \ldots, \delta_i - 2$ for all $\boldsymbol{x}$ in the neighbourhood $\mathcal{N}$ of $\bar{\boldsymbol{x}}$,

(B) $L_{\boldsymbol{g}_j} L_{\boldsymbol{f}}^{\delta_i - 1} h_i(\boldsymbol{x}) \neq 0$, $j = 1, \ldots, m$, $i = 1, \ldots, m$ for at least one j and all $\boldsymbol{x}$ in the neighbourhood $\mathcal{N}$ of $\bar{\boldsymbol{x}}$ and

(C) the $(m \times m)$ decoupling matrix

$$\boldsymbol{D}(\boldsymbol{x}) = \begin{bmatrix} L_{\boldsymbol{g}_1} L_{\boldsymbol{f}}^{\delta_1 - 1} h_1(\boldsymbol{x}) & L_{\boldsymbol{g}_2} L_{\boldsymbol{f}}^{\delta_1 - 1} h_1 & \ldots & L_{\boldsymbol{g}_m} L_{\boldsymbol{f}}^{\delta_1 - 1} h_1(\boldsymbol{x}) \\ L_{\boldsymbol{g}_1} L_{\boldsymbol{f}}^{\delta_2 - 1} h_2(\boldsymbol{x}) & L_{\boldsymbol{g}_2} L_{\boldsymbol{f}}^{\delta_2 - 1} h_2 & \ldots & L_{\boldsymbol{g}_m} L_{\boldsymbol{f}}^{\delta_2 - 1} h_2(\boldsymbol{x}) \\ \vdots & \vdots & \ddots & \vdots \\ L_{\boldsymbol{g}_1} L_{\boldsymbol{f}}^{\delta_m - 1} h_m(\boldsymbol{x}) & L_{\boldsymbol{g}_2} L_{\boldsymbol{f}}^{\delta_m - 1} h_m & \ldots & L_{\boldsymbol{g}_m} L_{\boldsymbol{f}}^{\delta_m - 1} h_m(\boldsymbol{x}) \end{bmatrix} \tag{4.4}$$

is non-singular for $\boldsymbol{x} = \bar{\boldsymbol{x}}$.

The time derivatives of a single output y_j are

$$\begin{aligned}
y_j &= h_j(\boldsymbol{x}) \\
\dot{y}_j &= L_{\boldsymbol{f}} h_j(\boldsymbol{x}) + \underbrace{L_{\boldsymbol{g}_1} h_j(\boldsymbol{x})}_{=0} u_1 + \cdots + \underbrace{L_{\boldsymbol{g}_m} h_j(\boldsymbol{x})}_{=0} u_m \\
\ddot{y}_j &= L_{\boldsymbol{f}}^2 h_j(\boldsymbol{x}) + \underbrace{L_{\boldsymbol{g}_1} L_{\boldsymbol{f}} h_j(\boldsymbol{x})}_{=0} u_1 + \cdots + \underbrace{L_{\boldsymbol{g}_m} L_{\boldsymbol{f}} h_j(\boldsymbol{x})}_{=0} u_m \\
&\vdots \\
y_j^{(\delta_j - 1)} &= L_{\boldsymbol{f}}^{\delta_j - 1} h_j(\boldsymbol{x}) + \underbrace{L_{\boldsymbol{g}_1} L_{\boldsymbol{f}}^{\delta_j - 2} h_j(\boldsymbol{x})}_{=0} u_1 + \cdots + \underbrace{L_{\boldsymbol{g}_m} L_{\boldsymbol{f}}^{\delta_j - 2} h_j(\boldsymbol{x})}_{=0} u_m \\
y_j^{(\delta_j)} &= L_{\boldsymbol{f}}^{\delta_j} h_j(\boldsymbol{x}) + L_{\boldsymbol{g}_1} L_{\boldsymbol{f}}^{\delta_j - 1} h_j(\boldsymbol{x}) u_1 + \cdots + L_{\boldsymbol{g}_m} L_{\boldsymbol{f}}^{\delta_j - 1} h_j(\boldsymbol{x}) u_m.
\end{aligned} \tag{4.5}$$

For all outputs, one obtains

$$\begin{bmatrix} y_1^{(\delta_1)} \\ \vdots \\ y_{m-1}^{(\delta_{m-1})} \\ y_m^{(\delta_m)} \end{bmatrix} = \underbrace{\begin{bmatrix} \boldsymbol{L}_{\boldsymbol{f}}^{(\delta_1)} h_1(\boldsymbol{x}) \\ \vdots \\ \boldsymbol{L}_{\boldsymbol{f}}^{(\delta_{m-1})} h_{m-1}(\boldsymbol{x}) \\ \boldsymbol{L}_{\boldsymbol{f}}^{(\delta_m)} h_m(\boldsymbol{x}) \end{bmatrix}}_{\boldsymbol{b}(\boldsymbol{x})} + \boldsymbol{D}(\boldsymbol{x}) \underbrace{\begin{bmatrix} u_1 \\ \vdots \\ u_{m-1} \\ u_m \end{bmatrix}}_{\boldsymbol{u}}. \tag{4.6}$$

Furthermore, the **synthetic input**

$$\boldsymbol{v} = \begin{bmatrix} v_1 \\ \vdots \\ v_{m-1} \\ v_m \end{bmatrix} = \begin{bmatrix} y_1^{(\delta_1)} \\ \vdots \\ y_{m-1}^{(\delta_{m-1})} \\ y_m^{(\delta_m)} \end{bmatrix}. \tag{4.7}$$

has to be defined for complete input-output linearization. This leads to a linear system with m integrator chains of lengths δ_j, where $j = 1, \ldots, m$. After designing a controller for the feedback linearized system and the synthetic input $\boldsymbol{v}$ with well-established linear control methods, the real input $\boldsymbol{u}$ is obtained by transforming the the system back. This can be achieved by inverting Equation 4.6, thus

$$\boldsymbol{u} = \boldsymbol{D}^{-1}(\boldsymbol{x})(\boldsymbol{v} - \boldsymbol{b}(\boldsymbol{x})). \tag{4.8}$$

A system has **full relative degree**, if $\delta = \sum_{j=1}^{m} \delta_j = n$, then the transformed system with the transformed states $\boldsymbol{z}$ becomes

$$\boldsymbol{z} = \begin{bmatrix} z_1 \\ \vdots \\ z_n \end{bmatrix} = \begin{bmatrix} \xi_{1,1} \\ \xi_{1,2} \\ \vdots \\ \xi_{1,\delta_1} \\ \xi_{2,1} \\ \vdots \\ \xi_{2,\delta_2} \\ \vdots \\ \xi_{m,1} \\ \vdots \\ \xi_{m,\delta_m} \end{bmatrix} = \boldsymbol{t}(\boldsymbol{x}) = \begin{bmatrix} h_1(\boldsymbol{x}) \\ L_{\boldsymbol{f}} h_1(\boldsymbol{x}) \\ \vdots \\ L_{\boldsymbol{f}}^{\delta_1 - 1} h_1(\boldsymbol{x}) \\ h_2(\boldsymbol{x}) \\ \vdots \\ L_{\boldsymbol{f}}^{\delta_2 - 1} h_2(\boldsymbol{x}) \\ \vdots \\ h_m(\boldsymbol{x}) \\ \vdots \\ L_{\boldsymbol{f}}^{\delta_m - 1} h_m(\boldsymbol{x}) \end{bmatrix} \tag{4.9}$$

with the diffeomorphism $\boldsymbol{t}(\boldsymbol{x})$ and the external linearizable states $\xi_{i,j}$. If the system does not have full relative degree, functions for the internal states $\{\eta_{\delta+1}, \ldots, \eta_n\}$ have to be found, so that $\boldsymbol{t}(\boldsymbol{x})$ becomes a local diffeomorphism. Then, the system can be separated in the external linearizable and controllable states $\xi_{i,j}$ and the internal non-controllable states η_i. For the internal states, that describe the internal dynamics of the system, stability has to be examined.

The linearized system for the states $[z_1, \ldots, z_\delta]^{\mathrm{T}}$can be written in the form

$$\begin{aligned} \dot{\boldsymbol{z}} &= \boldsymbol{A}\boldsymbol{z} + \boldsymbol{B}\boldsymbol{v} \\ \boldsymbol{y} &= \boldsymbol{C}\boldsymbol{z} \end{aligned} \tag{4.10}$$

with the system matrix $\boldsymbol{A}$, the input matrix $\boldsymbol{B}$ and the output matrix $\boldsymbol{C}$.

4.2 Feedforward control

For feedforward control, the ideal input $\boldsymbol{u}$ to obtain the desired system behavior is calculated by simulating the plant behaviour with the system model and the desired trajectories $\boldsymbol{y}_*$. No feedback from the physical plant is given to the controller. Consequently no model-plant mismatch can be considered. The block diagram of the feedforward controller is displayed in Figure 4.1.

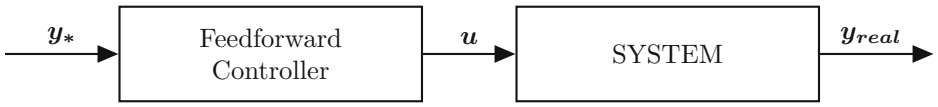

Figure 4.1: Block diagram for feedforward control. The desired output trajectories $\boldsymbol{y_*}$ are given to the controller and the ideal input $\boldsymbol{u}$ is calculated only by simulation. No feedback is given to the controller from the real plant. Therefore model-plant mismatch can not be accounted for.

4.3 Model predictive control with state estimation

The optimal input sequence for the finite controlled time horizon is found by an online minimization of a cost function based on predictions obtained by a process model. In general, model predictive control (MPC) leads to highly efficient control systems and is therefore used in various industrial fields and applications. The needed theory for the implementation of the MPC is given, a thorough definition can be found in [29]. The MPC is designed for a linear, time-discrete system in the form

$$\begin{aligned} \boldsymbol{z}(k+1) &= \boldsymbol{A_d}\boldsymbol{z}(k) + \boldsymbol{B_d}\boldsymbol{v}(k) \\ \boldsymbol{y}(k) &= \boldsymbol{C_d}\boldsymbol{z}(k) \end{aligned} \tag{4.11}$$

with the time-discrete state vector $\boldsymbol{z}(k)$ at time k, the system matrix $\boldsymbol{A_d}$, the input matrix $\boldsymbol{B_d}$, the time-discrete input vector $\boldsymbol{v}(k)$ at time k and the output matrix $\boldsymbol{C_d}$. Consequently the linear, time-invariant system obtained with the method of feedback linearization, must be discretized (subsection 4.3.1). The theory for the MPC algorithm (subsection 4.3.2) is given. The constraints on the physical inputs $\boldsymbol{u}$ must be mapped on the virtual inputs $\boldsymbol{v}$ (subsection 4.3.3). Furthermore, due to the difficulty to obtain real time data with high time resolution of the outputs and the states during the process, the basics of state estimation (subsection 4.3.4) are given.

4.3.1 Forward Euler method for discretizing continuous LTI state space models

The feedback linearized continuous LTI state space models must be discretized. The feedback linearized system consists of m integrator chains of length δ_i. Therefore the forward Euler method for discretizing is chosen, where every complex variable s of the Laplace-transformed continuous transfer function is replaced with $\frac{z-1}{T_s}$ with the sampling time T_s and the complex variable z of the z-transform. Consequently, the

linearized transfer function G_d is obtained from the continuous transfer function G by

$$G = \frac{Y_i(\mathrm{s})}{V_i(\mathrm{s})} = \frac{1}{\mathrm{s}^{\delta_i}} \rightarrow G_d = \frac{Y_i(\mathrm{z})}{V_i(\mathrm{z})} = \left(\frac{T_s}{\mathrm{z}-1}\right)^{\delta_i} = \left(\frac{T_s \mathrm{z}^{-1}}{1-\mathrm{z}^{-1}}\right)^{\delta_i} \tag{4.12}$$

with the Laplace transformed synthetic input V_i, the Laplace transformed output Y_i. If all $\delta_i = 1$, then

$$(1-\mathrm{z}^{-1})Y_i(\mathrm{z}) = T_s \mathrm{z}^{-1} V_i(\mathrm{z}) \rightarrow y_i(k+1) = y_i(k) + v_i(k) \tag{4.13}$$

and the time-discrete LTI system becomes

$$\begin{aligned} \begin{bmatrix} z_1(k+1) \\ \vdots \\ z_m(k+1) \end{bmatrix} &= \boldsymbol{I}_m \begin{bmatrix} z_i(k) \\ \vdots \\ z_m(k) \end{bmatrix} + \boldsymbol{I}_m \begin{bmatrix} v_i(k) \\ \vdots \\ v_m(k) \end{bmatrix} \\ \begin{bmatrix} y_1(k) \\ \vdots \\ y_m(k) \end{bmatrix} &= \boldsymbol{I}_m \begin{bmatrix} z_i(k) \\ \vdots \\ z_m(k) \end{bmatrix}. \end{aligned} \tag{4.14}$$

4.3.2 MPC algorithm and objective function

The algorithm chosen for the design and implementation of the MPC is generalized predictive control (GPC) in state-space formulation. For the MIMO system in Equation 4.11 with m inputs, m outputs and n states can be transformed in the augmented state space model

$$\begin{aligned} \begin{bmatrix} \boldsymbol{\Delta z}(k+1) \\ \boldsymbol{y}(k+1) \end{bmatrix} &= \begin{bmatrix} \boldsymbol{A_d} & \boldsymbol{0}^{\mathrm{T}} \\ \boldsymbol{C_d A_d} & \boldsymbol{I}_{m\times m} \end{bmatrix} \begin{bmatrix} \boldsymbol{\Delta z}(k) \\ \boldsymbol{y}(k) \end{bmatrix} + \begin{bmatrix} \boldsymbol{B_d} \\ \boldsymbol{C_d B_d} \end{bmatrix} \boldsymbol{\Delta v}(k) \\ \boldsymbol{y}(k) &= \begin{bmatrix} \boldsymbol{0} & \boldsymbol{I}_{m\times m} \end{bmatrix} \begin{bmatrix} \boldsymbol{\Delta z}(k) \\ \boldsymbol{y}(k) \end{bmatrix} \end{aligned} \tag{4.15}$$

with the $m \times m$ identity matrix $\boldsymbol{I}_{m\times m}$, the $m \times n$ zero matrix $\boldsymbol{0}$, the $n \times n$ system matrix $\boldsymbol{A_d}$, the $n \times m$ input matrix $\boldsymbol{B_d}$ and the $m \times n$ output matrix $\boldsymbol{C_d}$. The augmented state space model can be written in the form

$$\begin{aligned} \tilde{\boldsymbol{z}}(k+1) &= \tilde{\boldsymbol{A}}\tilde{\boldsymbol{z}}(k) + \tilde{\boldsymbol{B}}\boldsymbol{\Delta v}(k) \\ \boldsymbol{y}(k) &= \tilde{\boldsymbol{C}}\tilde{\boldsymbol{z}}(k) \end{aligned} \tag{4.16}$$

with the the augmented state vector $\tilde{\boldsymbol{z}}$, the augmented system $\tilde{\boldsymbol{A}}$, input $\tilde{\boldsymbol{B}}$ and output matrices $\tilde{\boldsymbol{C}}$. By defining the output matrix

$$\boldsymbol{Y} = \begin{bmatrix} \boldsymbol{y}(k+1|k)^{\mathrm{T}} & \boldsymbol{y}(k+2|k)^{\mathrm{T}} & \dots & \boldsymbol{y}(k+N_p|k)^{\mathrm{T}} \end{bmatrix}^{\mathrm{T}} \tag{4.17}$$

with the prediction horizon N_p, and the synthetic input matrix

$$\boldsymbol{\Delta V} = \begin{bmatrix} \boldsymbol{\Delta v}(k)^{\mathrm{T}} & \boldsymbol{\Delta v}(k+1)^{\mathrm{T}} & \dots & \boldsymbol{\Delta v}(k+N_c-1)^{\mathrm{T}} \end{bmatrix}^{\mathrm{T}} \tag{4.18}$$

with the control horizon N_c, one obtains

$$\boldsymbol{Y} = \boldsymbol{F}\tilde{\boldsymbol{z}}(k) + \boldsymbol{\Phi}\boldsymbol{\Delta V} \tag{4.19}$$

with the MPC system matrix

$$\boldsymbol{F} = \begin{bmatrix} \tilde{\boldsymbol{C}}\tilde{\boldsymbol{A}} & \tilde{\boldsymbol{C}}\tilde{\boldsymbol{A}}^2 & \dots & \tilde{\boldsymbol{C}}\tilde{\boldsymbol{A}}^{N_p} \end{bmatrix}^{\mathrm{T}} \tag{4.20}$$

and the MPC input matrix

$$\boldsymbol{\Phi} = \begin{bmatrix} \tilde{\boldsymbol{C}}\tilde{\boldsymbol{B}} & \boldsymbol{0} & \boldsymbol{0} & \dots & \boldsymbol{0} \\ \tilde{\boldsymbol{C}}\tilde{\boldsymbol{A}}\tilde{\boldsymbol{B}} & \tilde{\boldsymbol{C}}\tilde{\boldsymbol{B}} & \boldsymbol{0} & \dots & \boldsymbol{0} \\ \vdots & \vdots & \vdots & \ddots & \vdots \\ \tilde{\boldsymbol{C}}\tilde{\boldsymbol{A}}^{N_p-1}\tilde{\boldsymbol{B}} & \tilde{\boldsymbol{C}}\tilde{\boldsymbol{A}}^{N_p-2}\tilde{\boldsymbol{B}} & \tilde{\boldsymbol{C}}\tilde{\boldsymbol{A}}^{N_p-3}\tilde{\boldsymbol{B}} & \dots & \tilde{\boldsymbol{C}}\tilde{\boldsymbol{A}}^{N_p-N_c}\tilde{\boldsymbol{B}} \end{bmatrix}. \tag{4.21}$$

The cost function

$$\begin{aligned} J =& (\boldsymbol{Y}_* - \boldsymbol{Y})^{\mathrm{T}}\boldsymbol{Q}_y(\boldsymbol{Y}_* - \boldsymbol{Y}) + \boldsymbol{\Delta V}^{\mathrm{T}}\boldsymbol{R}\boldsymbol{\Delta V} \\ =& (\boldsymbol{Y}_* - \boldsymbol{Y})^{\mathrm{T}}\boldsymbol{Q}_y(\boldsymbol{Y}_* - \boldsymbol{Y}) \\ & - 2\boldsymbol{\Delta V}^{\mathrm{T}}\boldsymbol{\Phi}^{\mathrm{T}}\boldsymbol{Q}_y(\boldsymbol{Y}_* - \boldsymbol{Y}) + \boldsymbol{\Delta V}^{\mathrm{T}}(\boldsymbol{\Phi}^{\mathrm{T}}\boldsymbol{Q}_y\boldsymbol{\Phi} + \boldsymbol{R})\boldsymbol{\Delta V} \end{aligned} \tag{4.22}$$

with the output reference matrix $\boldsymbol{Y}_*$, the output weight matrix $\boldsymbol{Q}_y$ and the input weight matrix $\boldsymbol{R}$, can be formulated. By deriving the cost function with respect to $\boldsymbol{\Delta V}$ and setting it zero, the optimal input can be found by evaluating

$$\boldsymbol{\Delta V}(\boldsymbol{Y}_*, \boldsymbol{Y}) = (\boldsymbol{\Phi}^{\mathrm{T}}\boldsymbol{Q}_y\boldsymbol{\Phi} + \boldsymbol{R})^{-1}\boldsymbol{\Phi}^{\mathrm{T}}\boldsymbol{Q}_y(\boldsymbol{Y}_* - \boldsymbol{Y}). \tag{4.23}$$

4.3.3 Mapping of constraints

Possible constraints on the discrete system, such as

rate constraints $\quad \boldsymbol{\Delta v}^{\min} \leq \boldsymbol{\Delta v} \leq \boldsymbol{\Delta v}^{\max}$,

input constraints $\quad \boldsymbol{v}^{\min} \leq \boldsymbol{v} \leq \boldsymbol{v}^{\max}$

and output constraints $\quad \boldsymbol{y}^{\min} \leq \boldsymbol{y} \leq \boldsymbol{y}^{\max}$,

must be identified and considered by the MPC. For constrained problems, the objective of the MPC is to minimize the cost function while fulfilling the implemented inequalities leading to a quadratic programming problem. Constraints on the real inputs, namely

rate constraints $\quad \boldsymbol{\Delta u}^{\min} \leq \boldsymbol{\Delta u} \leq \boldsymbol{\Delta u}^{\max}$

and input constraints $\quad \boldsymbol{u}^{\min} \leq \boldsymbol{u} \leq \boldsymbol{u}^{\max}$,

must be mapped on the synthetic inputs $\boldsymbol{v}$ so that the physical boundaries of the system are considered. With Equation 4.8 and $\boldsymbol{v}(k) = \boldsymbol{v}(k-1) + \boldsymbol{\Delta v}(k)$, the constraints on $\boldsymbol{u}$ can be expressed as constraints on $\boldsymbol{\Delta v}(k)$. Consequently

$$\max(\mathbf{0}, \boldsymbol{D}(\boldsymbol{x}))\boldsymbol{u}^{\min} + \boldsymbol{b}(\boldsymbol{x}) - \boldsymbol{v}(k-1) \leq \boldsymbol{\Delta v}(k) \leq \min(\mathbf{0}, \boldsymbol{D}(\boldsymbol{x}))\boldsymbol{u}^{\max} + \boldsymbol{b}(\boldsymbol{x}) - \boldsymbol{v}(k-1) \quad \text{and}$$

$$\max(\mathbf{0}, \boldsymbol{D}(\boldsymbol{x}))\boldsymbol{\Delta u}^{\min} + \boldsymbol{b}(\boldsymbol{x}) \leq \boldsymbol{\Delta v}(k) \leq \min(\mathbf{0}, \boldsymbol{D}(\boldsymbol{x}))\boldsymbol{\Delta u}^{\max} + \boldsymbol{b}(\boldsymbol{x})$$

must be fulfilled.

4.3.4 State estimation

For the suggested control of the process, the outputs $\boldsymbol{y}$ of the system as well as the state vector $\boldsymbol{x}$ have to be known. However, all variables might not be measured or measurable. Therefore, by using an observer, the missing measurements can be estimated. The state estimator is implemented and designed independently of the MPC.

For the design of an extended Luenberger observer, the observability matrix

$$\boldsymbol{Q}(\boldsymbol{x}) = [h_1, \ldots, \boldsymbol{L}_{\boldsymbol{f}}^{m_1-1} h_1, \ldots, h_m, \ldots, \boldsymbol{L}_{\boldsymbol{f}}^{m_m-1} h_m]^{\mathrm{T}} \tag{4.24}$$

with the observability indices $\sum_{i=1}^{m} m_i = n$, must have rank n. Furthermore, the model of the observer

$$\dot{\hat{\boldsymbol{x}}} = \boldsymbol{f}(\boldsymbol{y_{meas}}, \hat{\boldsymbol{x}}, \boldsymbol{u_k}) + \boldsymbol{g}(\boldsymbol{h}^{-1}(\boldsymbol{y_{meas}}, \boldsymbol{u_k}) - \hat{\boldsymbol{x}}) \tag{4.25}$$

with the measured part $\boldsymbol{y_{meas}}$ and the unmeasured part $\hat{\boldsymbol{x}}$ can be formulated. With time, the estimation error shall approach zero, hence

$$\lim_{t \to \infty} |\hat{\boldsymbol{x}} - \boldsymbol{x}| = \mathbf{0}. \tag{4.26}$$

4.3.5 Block diagram

The block diagram for the MPC with state estimation is displayed in Figure 4.2. The control error $\boldsymbol{e}$ is the difference of the the desired output trajectories $\boldsymbol{y}_*$ and the measured or estimated output variables $\hat{\boldsymbol{y}}$. The optimization solver tries to minimize the objective function (Equation 4.22) by finding the optimal control sequence $\boldsymbol{v_k}$.

Furthermore, the physical constraints on $\boldsymbol{u_k}$ are considered by the nonlinear mapping on the synthetic input $\boldsymbol{v_k}$. After transforming the optimized synthetic input $\boldsymbol{v_k}$ into the real input $\boldsymbol{u_k}$ with the nonlinear transformation (Equation 4.8), the real inputs $\boldsymbol{u_k}$ can be applied to the physical plant. In the state estimator, the states and outputs that are not measured are estimated.

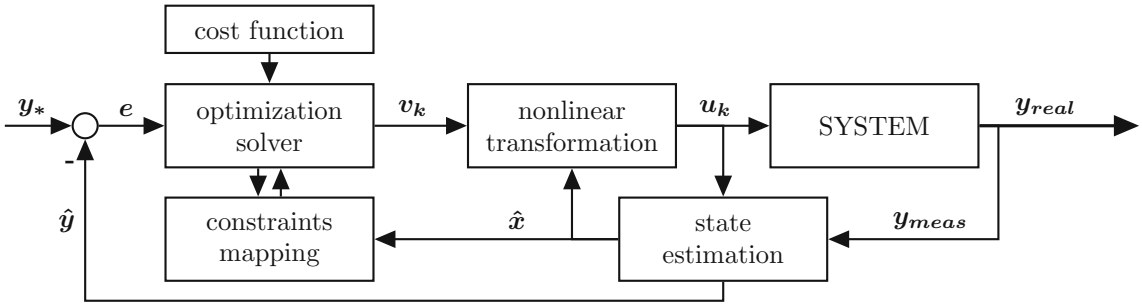

Figure 4.2: Block diagram for model predictive control. The control error $\boldsymbol{e}$ is calculated as the difference of the desired output trajectory $\boldsymbol{y_*}$ and the measured or estimated output vector $\hat{\boldsymbol{y}}$. The cost function is minimized while simultaneously considering the constraints of the system by the optimization solver. The resulting control sequence of the synthetic input $\boldsymbol{v_k}$ is transformed into the real input vector $\boldsymbol{u_k}$, which is then applied to the plant. States and outputs that are not measured are estimated in the state estimator.

Chapter 5

Control applied

The state space model

$$\dot{\boldsymbol{x}} = \underbrace{\begin{bmatrix} 0 \\ \mu c_X \\ -q_G c_X \\ -q_M c_X \\ -q_T c_X \end{bmatrix}}_{\boldsymbol{f}(\boldsymbol{x})} + \underbrace{\begin{bmatrix} 1 & 1 & 1 & -1 & -1 \\ -\frac{c_X}{V_R} & -\frac{c_X}{V_R} & -\frac{c_X}{V_R} & \frac{c_X}{V_R} & 0 \\ \frac{c_{G,S}-c_G}{V_R} & \frac{c_{G,B}-c_G}{V_R} & \frac{-c_G}{V_R} & 0 & 0 \\ \frac{c_{M,S}-c_M}{V_R} & \frac{c_{M,B}-c_M}{V_R} & \frac{-c_M}{V_R} & 0 & 0 \\ -\frac{c_T}{V_R} & -\frac{c_T}{V_R} & \frac{c_{T,N}-c_T}{V_R} & 0 & 0 \end{bmatrix}}_{\boldsymbol{g}(\boldsymbol{x})} \underbrace{\begin{bmatrix} \dot{V}_S \\ \dot{V}_B \\ \dot{V}_N \\ \dot{V}_H \\ \dot{V}_{BL} \end{bmatrix}}_{\boldsymbol{u}} \tag{5.1}$$

$$\boldsymbol{y} = \boldsymbol{h}(\boldsymbol{x}) = [V_R, c_X, \mu, c_M, c_T]^{\mathrm{T}}$$

with the state vector $\boldsymbol{x} = [V_R, c_X, c_G, c_M, c_T]^{\mathrm{T}}$ and the inputs $\boldsymbol{u} = [\dot{V}_S, \dot{V}_B, \dot{V}_N, \dot{V}_H, \dot{V}_{BL}]^{\mathrm{T}}$ can be derived from the equations in chapter 3. With

the biomass specific glucose uptake	$q_G = q_{G,max}\frac{c_G}{c_G+K_{S,G}}$,
the biomass specific mannose uptake	$q_M = q_{M,max}\frac{c_M}{c_M+\frac{K_{S,M}}{K_{S,G}}c_G+K_{S,M}}$,
the biomass specific growth rate	$\mu = Y_{X/G}q_G + Y_{X/M}q_M$
and the biomass specific nutrient uptake	$q_T = \frac{\mu}{Y_{X/T}}$

the system is fully defined. With the theory given in chapter 4, the nonlinear, time continuous system is feedback linearized and a feedforward controller and an MPC with state estimation are designed.

5.1 Feedback linearized model

Based on the theory given in section 4.1, the state space model is linearized. The system has full relative degree $\delta = 5 = \{1, 1, 1, 1, 1\}$ and the decoupling matrix becomes

$$\boldsymbol{D}(\boldsymbol{x}) = \frac{1}{V_R} \begin{bmatrix} V_R & V_R & V_R & -V_R & -V_R \\ -c_X & -c_X & -c_X & c_X & 0 \\ \Delta_{M,S}a_1 - \Delta_{G,S}a_2 & \Delta_{M,B}a_1 - \Delta_{G,B}a_2 & c_G a_2 - c_M a_1 & 0 & 0 \\ \Delta_{M,S} & \Delta_{M,B} & -c_M & 0 & 0 \\ -c_T & -c_T & (c_{T,N} - c_T) & 0 & 0 \end{bmatrix} \tag{5.2}$$

with

$$\begin{aligned} a_1 &= Y_{X/M} \frac{q_{M,max} - q_M}{K_{S,M} + c_M + \frac{K_{S,M}}{K_{S,G}} c_G} \\ a_2 &= \frac{K_{S,M}}{K_{S,G}} Y_{X/M} \frac{q_M}{K_{S,M} + c_M + \frac{K_{S,M}}{K_{S,G}} c_G} - Y_{X/G} \frac{q_{G,max} - q_G}{K_{S,G} + c_G} \end{aligned} \tag{5.3}$$

and

$$\begin{aligned} \Delta_{G,S} &= (c_{G,S} - c_G) \quad \Delta_{M,S} = (c_{M,S} - c_M) \\ \Delta_{G,B} &= (c_{G,B} - c_G) \quad \Delta_{M,B} = (c_{M,B} - c_M). \end{aligned} \tag{5.4}$$

The external dynamics of the linearized system

$$\dot{\boldsymbol{z}} = \underbrace{\begin{bmatrix} 0 \\ \mu c_X \\ (a_2 q_G - a_1 q_M) c_X \\ -q_M c_X \\ -q_T c_X \end{bmatrix}}_{\boldsymbol{b}(\boldsymbol{x})} + \boldsymbol{D}(\boldsymbol{x})\boldsymbol{u} \tag{5.5}$$

with the state vector $\boldsymbol{z} = \boldsymbol{y} = [V_R, c_X, \mu, c_M, c_T]^{\mathrm{T}}$ are obtained. With the definition of the synthetic input $\boldsymbol{v} = \boldsymbol{y} = [\dot{V}_R, \dot{c}_X, \dot{\mu}, \dot{c}_M, \dot{c}_T]^{\mathrm{T}}$, the input-output linearized system

$$\begin{aligned} \dot{\boldsymbol{z}} &= \boldsymbol{I}_5 \boldsymbol{v} \\ \boldsymbol{y} &= \boldsymbol{I}_5 \boldsymbol{z} \end{aligned} \tag{5.6}$$

is obtained with the 5×5 identity matrix $\boldsymbol{I}_5$. The real inputs are obtained with

$$\boldsymbol{u} = \boldsymbol{D}^{-1}(\boldsymbol{x})(\boldsymbol{v} - \boldsymbol{b}(\boldsymbol{x})). \tag{5.7}$$

5.2 Feedforward control

In analogy to the block diagram for feedforward control (Figure 4.1), the controller is implemented with the feedback linearized model.

5.3 MPC with feedback linearization and state estimation

The linearized system

$$\begin{aligned} \dot{\boldsymbol{z}} &= \boldsymbol{I}_5 \boldsymbol{v} \\ \boldsymbol{y} &= \boldsymbol{I}_5 \boldsymbol{z} \end{aligned} \tag{5.8}$$

is discretized to

$$\begin{aligned} \boldsymbol{z}(k+1) &= \boldsymbol{I}_5 \boldsymbol{z}(k) + \boldsymbol{I}_5 \boldsymbol{v}(k) \\ \boldsymbol{y}(k) &= \boldsymbol{I}_5 \boldsymbol{z}(k) \end{aligned} \tag{5.9}$$

with $T_s = 1\text{h}$ for which the MPC is implemented according to the given theory in section 4.3. The constraints on the physical inputs $\boldsymbol{u}$ and the states $\boldsymbol{z}$ are formulated (Table 5.1) with a control horizon N_c of five hours and a prediction horizon N_p of ten hours. For the MPC strategy, measurements or estimations of the reactor volume V_R, the biomass concentration c_X, the biomass specific growth rate μ, the glucose concentration c_G, the mannose concentration c_M and the nutrient concentration c_T are needed. Different measurements scenarios are examined.

By increasing the amount of estimated state variables, measurement expenses can be reduced. Especially the concentrations of the liquid phase inside the reactor, namely the biomass, glucose, mannose and nutrient concentration, can be difficult to measure with a sufficiently small sampling time. Depending on the experimental setup, different measurement strategies and sampling times may be possible. The following three measurement scenarios for the control of the process with MPC are examined, whereas the measurement expenses decrease with increasing strategy number.

Measurement strategy MPC1. All states and outputs are directly measurable. Although providing the most accurate information to the control algorithm, this strategy has the highest measurement expenses. The measurement vector can be written as

$$\boldsymbol{y_{meas}} = [V_R, c_X, c_G, c_M, c_T, \mu, \text{OUR}, \text{CER}]. \tag{5.10}$$

Table 5.1: Implemented constraints on the inputs and the linearized states. The constraints on the physical inputs and the linearized states are formulated. Due to their definition and the experimental setup, only positive values are valid.

	Lower Bound	Upper Bound	
$\dot{V}_S$	0	0.5	L/h
$\dot{V}_B$	0	0.3	L/h
$\dot{V}_T$	0	0.3	L/h
$\dot{V}_H$	0	0.5	L/h
$\dot{V}_{BL}$	0	0.5	L/h
V_R	0	5	L
c_X	0	∞	g/L
μ	0	0.3	g/L
c_M	0	$\max(c_{M,S}, c_{M,B})$	g/L
c_T	0	$c_{T,N}$	g/L

Measurement strategy MPC2. The reactor volume, offgas signal and sugar concentrations can be measured. The biomass concentration, the biomass specific uptake and the nutrient concentration are estimated. The measurement vector can be written as

$$\boldsymbol{y_{meas}} = [V_R, c_G, c_M, \text{OUR}, \text{CER}]. \tag{5.11}$$

Measurement strategy MPC3. To minimize measurement expenses, only the reactor volume and the offgas measurements are measured. The biomass, sugar and nutrient concentration as well as the biomass specific uptake rate are estimated. The measurement vector can be written as

$$\boldsymbol{y_{meas}} = [V_R, \text{OUR}, \text{CER}]. \tag{5.12}$$

5.4 Implementation and integration into process control

The algorithms described are implemented in MATLAB 2020a to provide an independent simulation environment. In this environment, the system behaviour, controller performance and stability of the system can be examined (chapter 6). Furthermore the process control strategy is implemented and integrated in the existing online data processing tool in MATLAB 2020a. Via an OPC server, the measurements stored at the process information management system (PIMS) are obtained. Then the data is processed in MATLAB 2020a and the inputs for the next time steps are calculated. The calculated inputs are then given back to the PIMS so that the pumps for the feed can be adjusted accordingly. A more detailed explanation of the process control structure can be found in chapter 2. The implemented control strategy is then used for the conducted experiments in chapter 7.

Chapter 6

Simulations

By simulating the system behaviour in combination with the control algorithm, the system and controller performance is examined. First, possible and beneficial setpoints for the continuous process are identified under the assumption of a perfect model and constant feed concentrations (section 6.1). The resulting feed, harvest and bleed rates are discussed. The influence of changing kinetic parameters, feed concentrations and setpoitns are examined and visualized in section 6.2. The performance of the feedforward controller for varying kinetics and feed concentration deviations is examined (section 6.3). Furthermore the three different measuring and state estimation scenarios for the MPC as well as the feedforward controller are examined and analysed (section 6.4).

6.1 Setpoints, trajectory planning and controllability

As shown in chapter 5, the control of the system with five different inputs enables the control of five different outputs. However, due to the nonlinearities and the coupling of the states, not all setpoints are beneficial and certain setpoint combinations may not be feasible, for example very high sugar concentrations and small biomass growth rates contradict each other. Furthermore, the choice of the state of operation is also based on economical aspects during process design. The ratio of used SSL and BALI™ is of special interest in the examined process as the investment costs can be significantly reduced by minimizing BALI™ usage. Beneficial and feasible setpoints have to be identified.

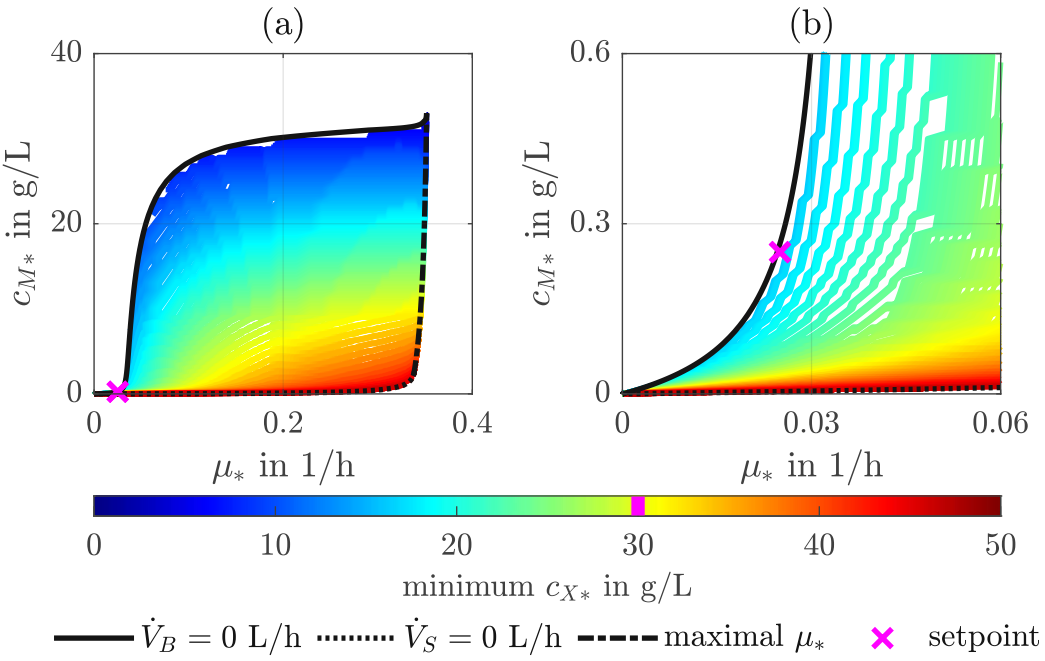

Figure 6.1: Possible setpoint combinations for c_{M*}, μ_* and c_{X*}. Limited by $\dot{V}_B = 0$ L/h, $\dot{V}_S = 0$ L/h and the maximal possible biomass growth rate μ, the feasibility plane for constant feed concentrations and $c_{T*} = 0.025$ g/L is displayed, whereas c_{X*} indicates the minimum biomass setpoint, so that $\dot{V}_H > 0$ L/h. The chosen setpoint combination for μ_* and c_{M*} is labeled. In subfigure (a) the whole plane is represented. In subfigure (b) the region of interest is enlarged.

The feasibility analysis for possible setpoint combinations is done under the assumption of a stable state and perfect model. By varying the setpoints against each other, namely the reactor volume V_{R*}, the biomass concentration c_{X*}, the specific growth rate μ_*, the mannose concentration c_{M*} and the nutrient concentration c_{T*}, and inserting in the control law (Equation 4.8), the feed, harvest and bleed rates in stable state are obtained. Note that the setpoint of the reactor volume is independent of the other setpoints and is solely a scaling factor. A setpoint combination is feasible if all system inputs assume positive values. Further limitations, such as a maximal dilution rate, a maximum flux thought the membrane module or maximal absolute biomass growth per hour due to limitations of the cooling system, can be considered for experimental design based on the characteristics of the experimental setup. In Figure 6.1 possible setpoint combinations for c_{X*}, μ_* and c_{M*} are displayed for a given setpoint c_{T*}. The possible setpoint combinations are limited by $\dot{V}_B$ and $\dot{V}_S$

becoming zero and the general possible kinetic behaviour (maximal possible μ due to model structure and parameters). The chosen setpoint combination for the subsequent simulations and studies is marked in Figure 6.1. The numerical values as well as the resulting feed rates in stable state can be found in Table 6.1.

Table 6.1: Identified beneficial setpoint combination and corresponding feedrates.

y_*	Value		u	Value	
V_{R*}	4	L	$\dot{V}_S$	170	mL/h
c_{X*}	30	g/L	$\dot{V}_B$	1	mL/h
μ_*	0.025	1/h	$\dot{V}_T$	25	mL/h
c_{M*}	0.25	g/L	$\dot{V}_H$	96	mL/h
c_{T*}	0.025	g/L	$\dot{V}_{BL}$	100	mL/h

6.2 Influence of parameters, feed concentrations and setpoints

The system behavior is described by the model structure and the kinetic parameters and can be influenced by the feed, harvest and bleed rates as well as the concentrations in the feed. All these factors are coupled with each other. The influence of changing kinetic parameters and feed concentrations as well as the impact of the choice of the setpoints is examined. By varying the parameters to $\pm 25\%$ and $\pm 10\%$ of their original value, their influence is displayed.

Influence of setpoints (Figure 6.2). Changing the setpoint for the reactor volume V_{R*} increases and decreases the inputs accordingly. However, the ratios between the different feeds stay constant. A higher biomass setpoint leads to an increased demand of sugars and nutrients. As the kinetics are biomass specific, the three feeds increase. The bleed rate can be kept constant and the harvest rate must be changed accordingly. The change in demand of sugars for varying μ_* is mainly accounted for by changing the BALI™ feedrate and consequently increasing glucose consumption. Changes of c_{M*} are realised by changing ratios of the SSL and BALI™ feed. Changes of c_{T*} correspond to small changes in the inputs.

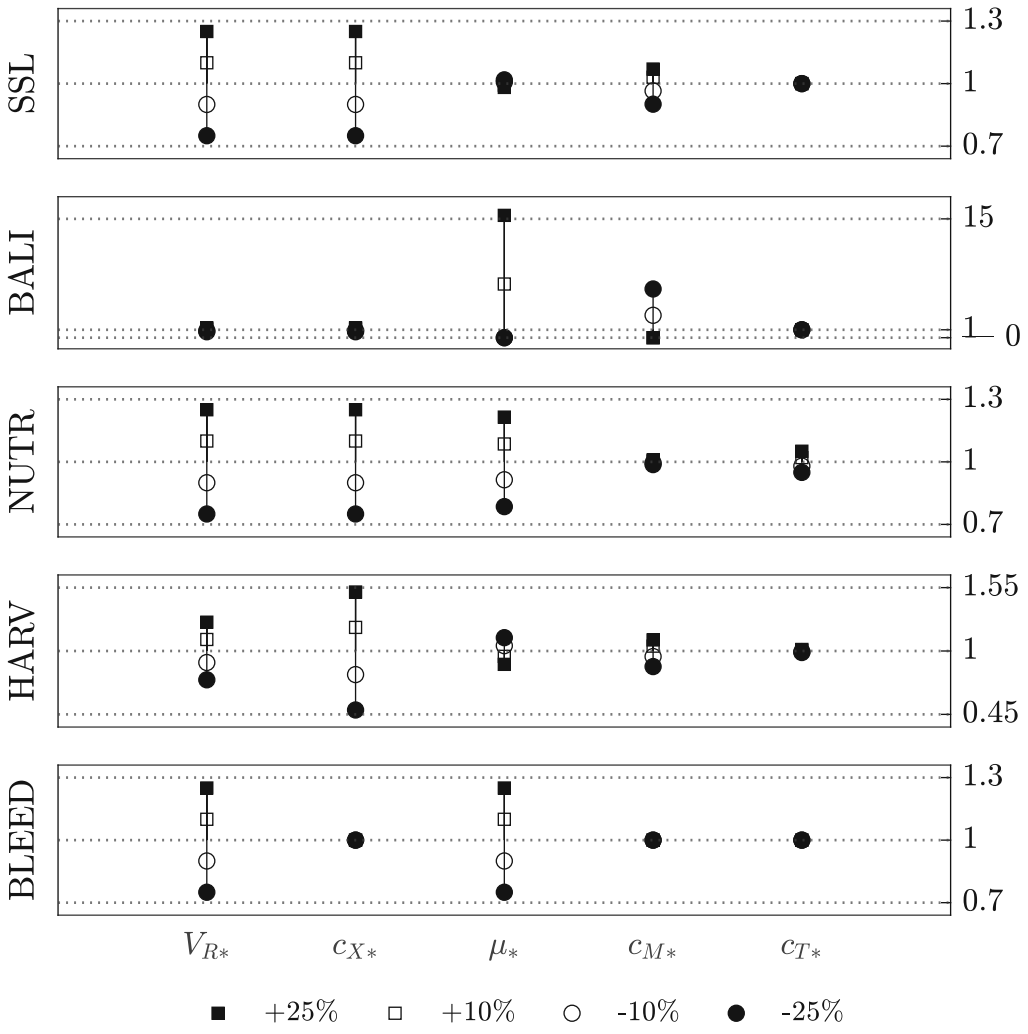

Figure 6.2: Influence of setpoint choice on feed, harvest and bleed rates. The relative influence of changing a single setpoint to ± 25% and ± 10% of its value in Table 6.1 on the feed, harvest and bleed rates (SSL, BALI, NUTR, HARV and BLEED) is examined.

Influence of feed concentrations (Figure 6.3). Changes of the glucose concentrations in the SSL are accounted for by changes in the BALI™ feed. If the mannose concentration in the SSL changes significantly, the BALI™ as well as the harvest rate have to be adjusted so that the process can maintain the same setpoint. Changes of the concentrations in BALI™ have less impact on the process, however to use BALI™ effectively, the glucose concentration in BALI™ is of high importance. Changes in the nutrient solution mainly influence the addition of nutrients.

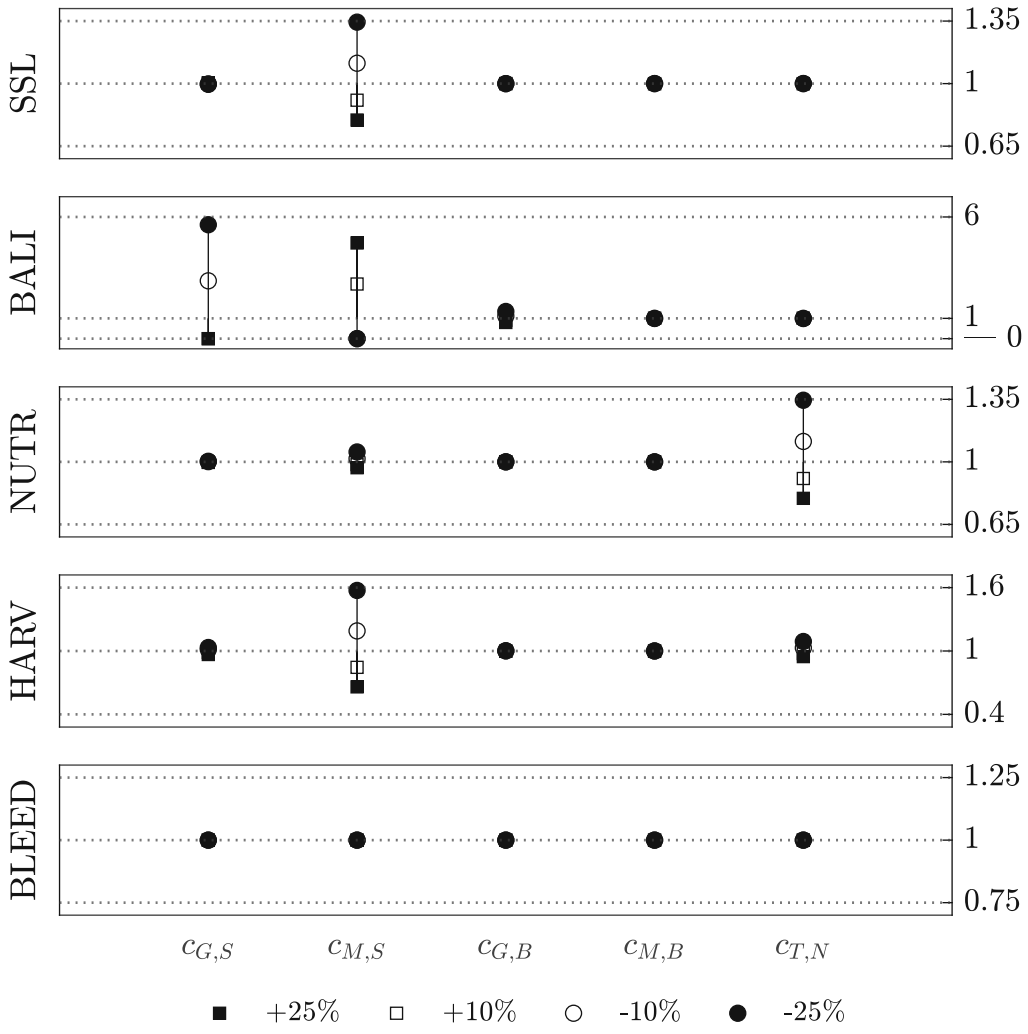

Figure 6.3: Influence of feed concentrations on feed, harvest and bleed rates. The influence of varying feed concentration (± 25% and ± 10%) on the feed, harvest and bleed rates (SSL, BALI, NUTR, HARV and BLEED) is examined.

Influence of kinetic parameters (Figure 6.4). Changing the kinetic parameters for the glucose uptake ($q_{G,max}$, $K_{S,G}$) has little effect on the calculated ideal input rates compared to the parameters for mannose uptake. With increased maximal mannose uptake, the ratio between BALI™ and SSL becomes smaller, making the process more economical. If the mannose uptake is decreased, more BALI™ must be added to achieve the desired setpoints. Discrepancies of all yields have a significant effect on the process and therefore must be determined precisely.

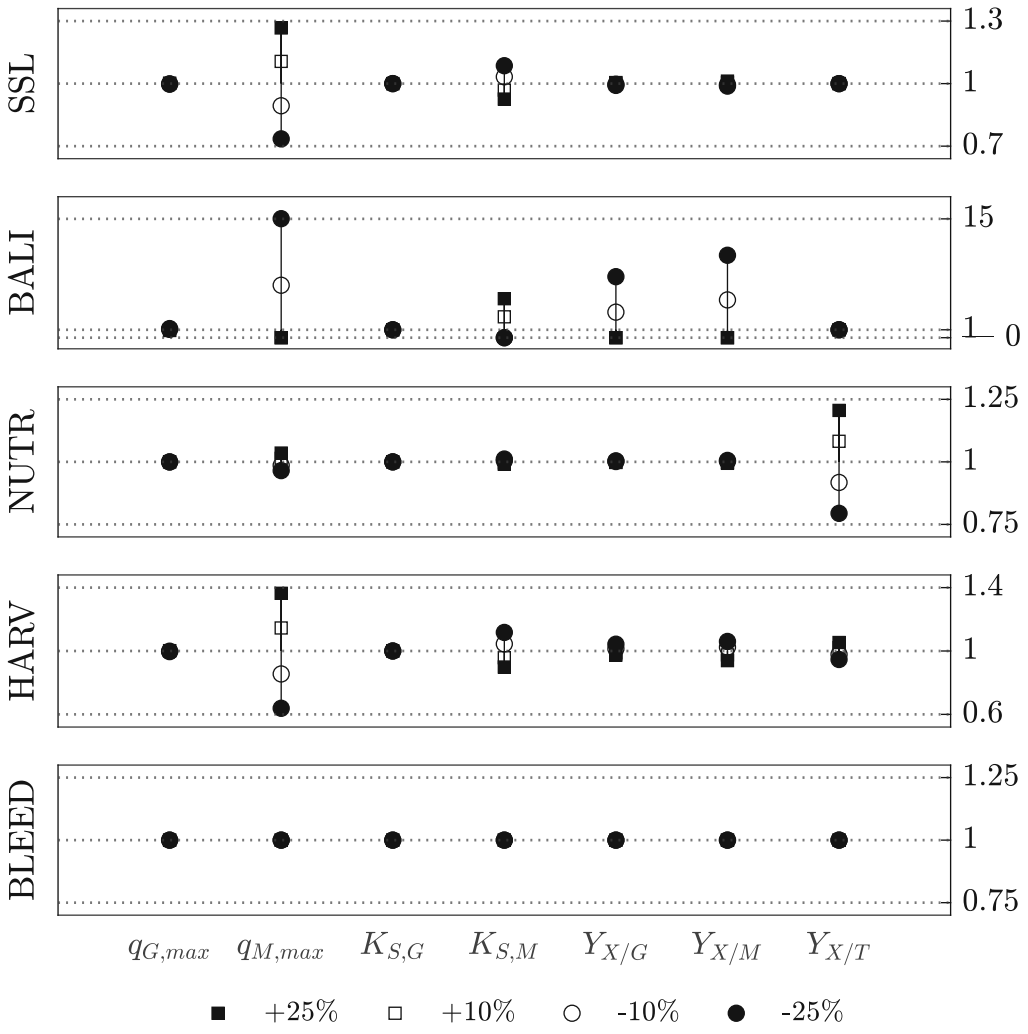

Figure 6.4: Influence of kinetic parameters on feed, harvest and bleed rates. The influence of changing kinetic parameters (± 25% and ± 10%) on the feed, harvest and bleed rates (SSL, BALI, NUTR, HARV and BLEED) is examined.

6.3 Feedforward control

For feedforward control, the feed, harvest and bleed rates for the ideal controller (Table 6.1) are applied to the system. The system behavior is simulated with deviating parameters. A stable state for all simulations with the deflected system was reached. However in general, the outputs of the system deviate from the chosen setpoints.

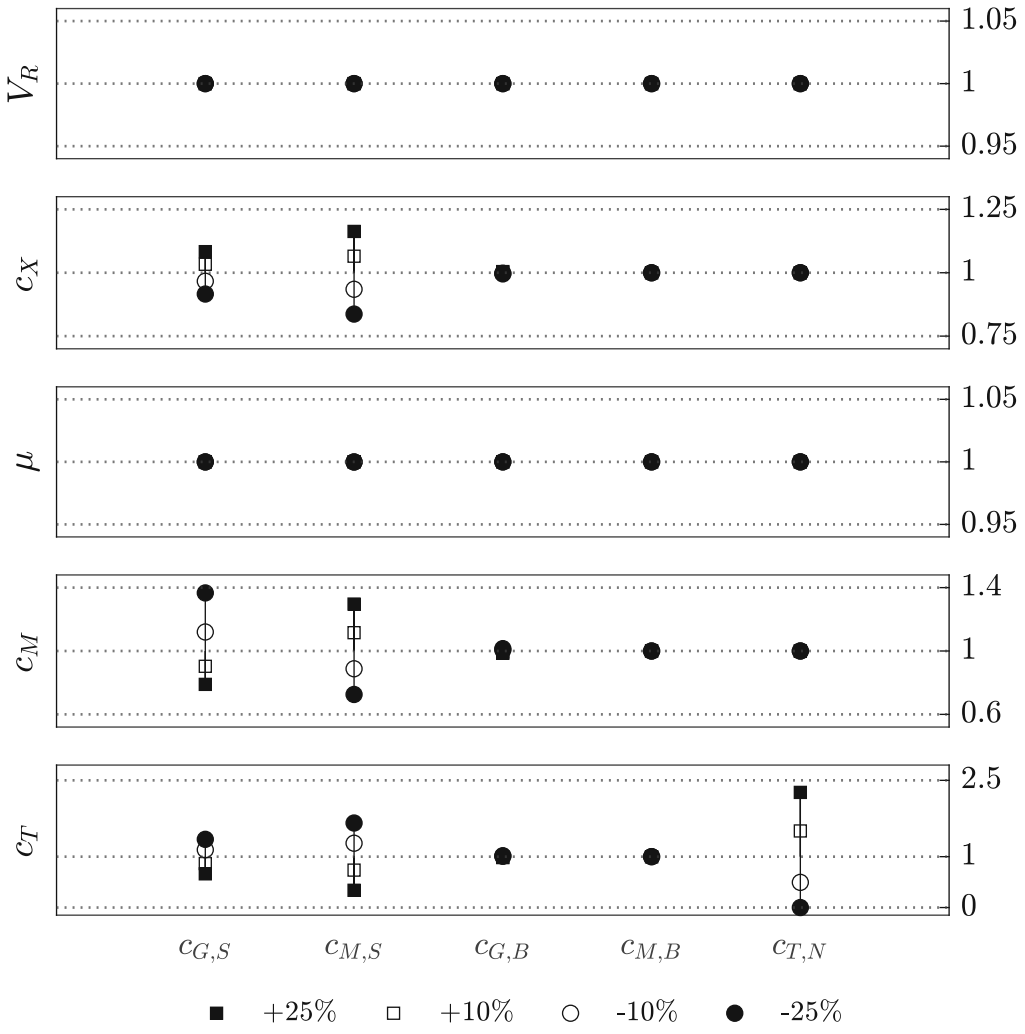

Figure 6.5: Influence of feed concentrations on outputs for feedforward control. The influence of changing feed concentrations (± 25% and ± 10%) on the outputs for feedforward control is examined.

Influence of feed concentrations (Figure 6.5). V_R and μ are not influenced by changing feed concentrations. However, the concentrations in the reactor vary. Especially the concentrations in the SSL are of special interest. Increasing sugar concentrations lead to higher biomass concentrations. If the glucose concentration in the SSL is increased, the higher biomass leads to more mannose consumption and the mannose concentration in the reactor decreases. Higher mannose concentration in the feed lead to higher mannose concentrations in the bioreactor due to accumulation.

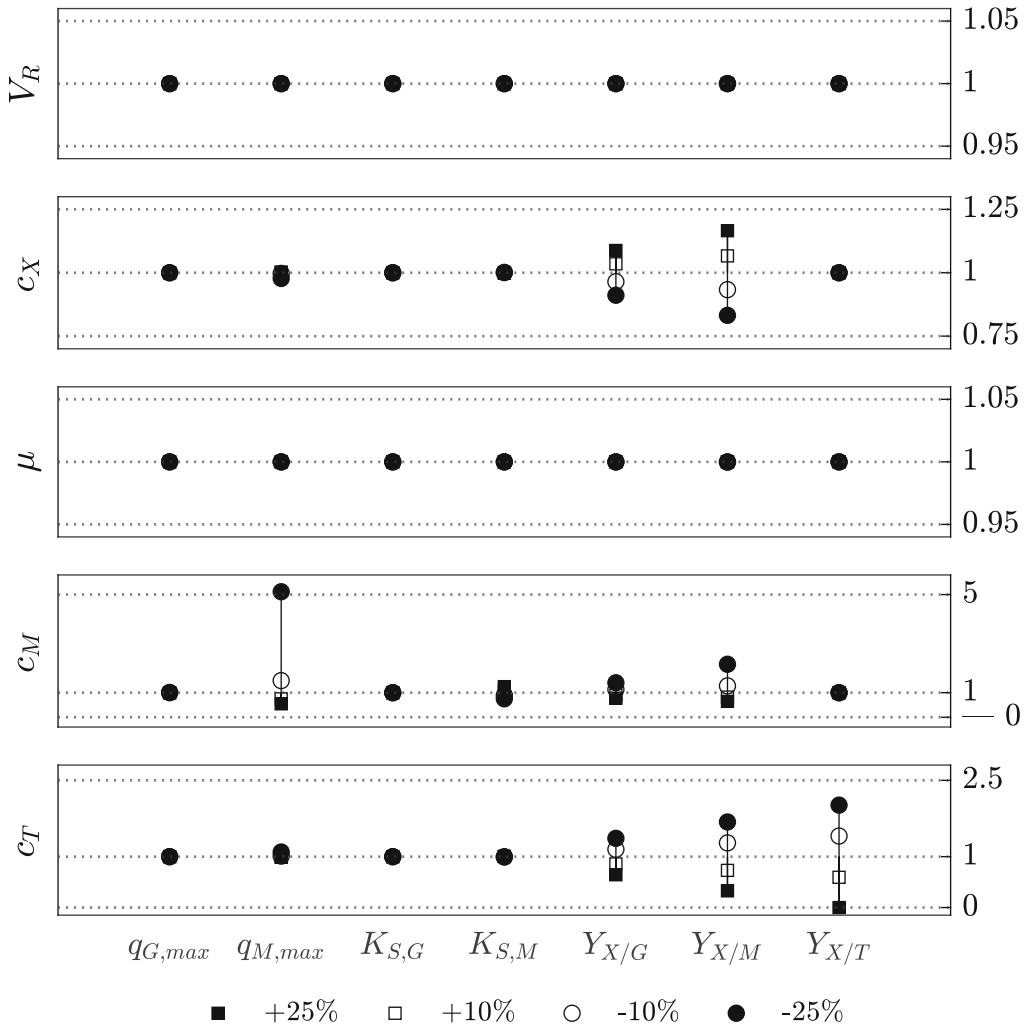

Figure 6.6: Influence of kinetic parameters on outputs for feedforward control. The influence of changing kinetic parameters ($\pm$ 25% and $\pm$ 10%) on the outputs for feedforward control is examined.

The nutrient concentration drops, if the biomass concentration increases as more nutrients are consumed.

Influence of single parameters (Figure 6.6). V_R and μ are not influenced by changing kinetic parameters. Changing kinetics for the glucose uptake have little impact on the system. Especially a decrease of the maximal mannose uptake $q_{M,max}$ would lead to a significant accumulation of mannose. Decreasing yields lead to smaller biomass concentration and therefore a smaller sugar demand. The mannose accumulates.

6.4 Comparison of measuring strategies for the MPC

In order to estimate the control performance as well as the accuracy of the state estimation under real conditions for the MPC measuring scenarios and the feedforward controller, the system behavior is simulated with deviating kinetic parameters (multiplied with random normally distributed factors where $\mu = 1$ and $\sigma = 0.05$). In Table 6.2, the measurement and state estimation scenarios are summarized.

Table 6.2: Examined measurement and state estimation strategies. For the different strategies, namely feedforward control (FF) and MPC1, MPC2 and MPC3, different quantities are measured and processed during the fermentation. While no feedback is given to the control algorithm for feedforward control, different signals are evaluated for the MPC strategies.

	V_R	c_X	c_G	c_M	c_T	μ	OUR	CER
FF	×	×	×	×	×	×	×	×
MPC1	■	■	■	■	■	■	■	■
MPC2	■	□	■	■	□	□	■	■
MPC3	■	□	□	□	□	□	■	■

× unknown ■ measured □ estimated

In Figure 6.7 the results of five hundred simulations per strategy are shown. For feedforward control (FF), the reactor volume V_R and the biomass specific growth rate μ can be controlled with little to no control error. However deviations from the concentrations in the reactor, namely the biomass concentration c_X, the mannose concentration c_M and the nutrient concentration c_T, are not measured and are therefore not accounted for. Furthermore, since no feedback is given to the control algorithm, other deviations and disturbances are not considered.

With minimal measurements as for MPC3 (V_R, OUR and CER), the control errors for the biomass concentration can be reduced significantly. Moreover, system disturbances are detected and the control action can be adapted accordingly. However, control errors for mannose and nutrient concentration are approximately the same for

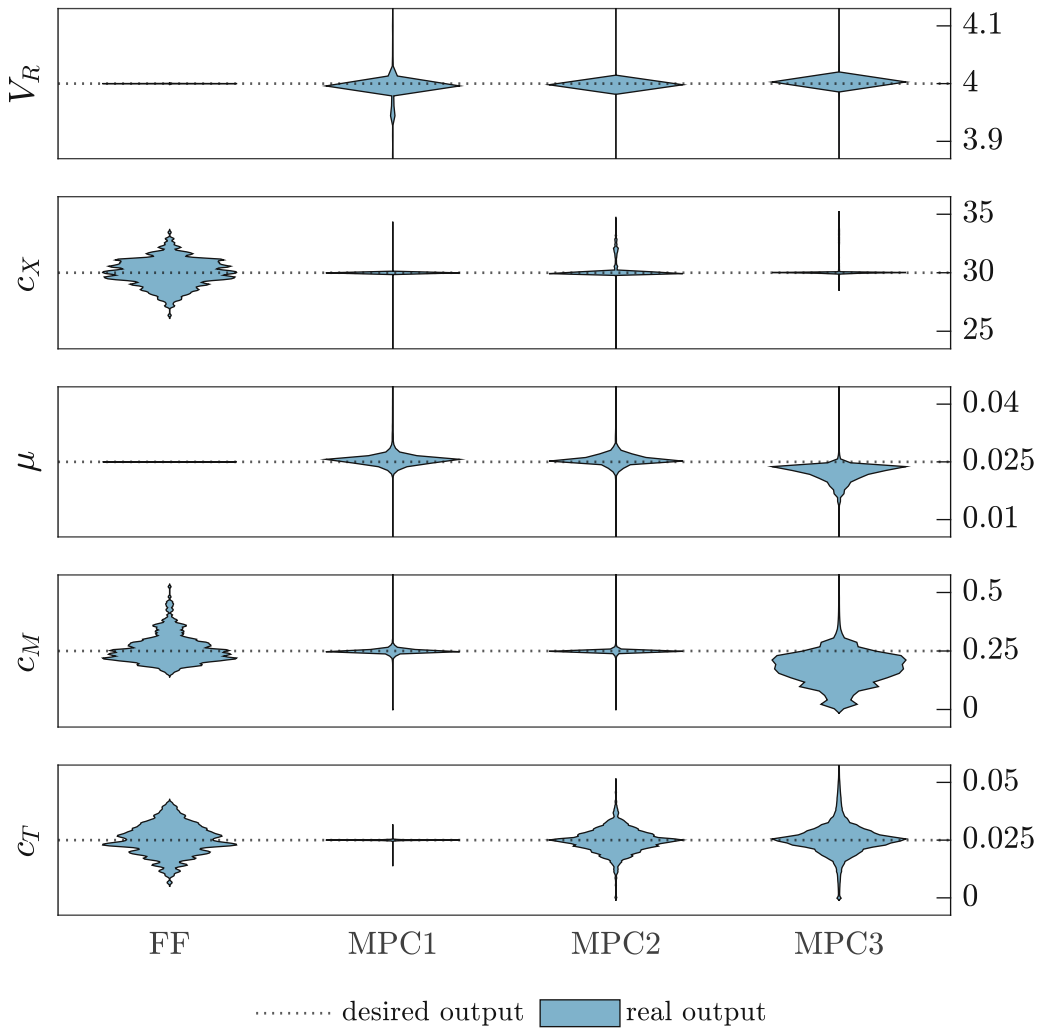

Figure 6.7: Performance of control strategies for deviating system behavior. Deviating system behavior is simulated with deviating kinetic parameters, which are multiplied with random normally distributed factors ($\mu = 1$ and $\sigma = 0.05$). The distribution of the obtained outputs are presented for the five output variables as well as for the implemented control strategies.

FF and MPC3. By including further measurements of the mannose concentration in the reactor (MPC2), the control error for the mannose concentration can be reduced significantly compared to MPC3. Measuring all state variables and output variables (MPC1) leads to the smallest control errors. However, the measuring expenses are

the highest. In Table 6.3 the root mean square errors (RMSE) for the estimation and control errors are calculated.

Table 6.3: Results of simulation for Feedforward control and MPC. The kinetic parameters of the system are deviated (with a normally distributed factor with $\mu = 1$ and $\sigma = 0.05$). The results of 500 simulations per control strategies are quantified by the RMSE (root mean square error) for the estimation and control performance.

		FF	MPC1	MPC2	MPC3
Estimation errors $\sqrt{\frac{1}{n}\sum_i^n(\hat{\boldsymbol{y}} - \boldsymbol{y_{real}})^2}$	V_R	×	■	■	■
	c_X	×	■	0.0267	0.0328
	μ	×	■	4.33e-05	5.76e-4
	c_M	×	■	■	0.1046
	c_T	×	■	0.0051	0.0050
Control errors $\sqrt{\frac{1}{n}\sum_i^n(\boldsymbol{y_*} - \boldsymbol{y_{real}})^2}$	V_R	0.0	0.1053	0.1178	0.2366
	c_X	1.125	0.6144	0.6853	1.0100
	μ	0.0	0.0181	0.0162	0.0188
	c_M	0.1531	0.0275	0.0303	0.1172
	c_T	0.0080	0.0002	0.0051	0.0068

× no feedback to controller ■ measured variable

Chapter 7

Experiments

A first experimental run with feedforward control was carried out to test the real system behaviour as well as the potential of the suggested control strategy at the facilities of TU Wien - Institute of Chemical, Environmental and Bioscience Engineering. The bioreactor and equipment is set up according to chapter 2. By adapting the feed, harvest and bleed rates, the examined system shall be controlled so that a stable state is reached. The five controlled variables, namely the reactor volume, the biomass, mannose and nutrition concentration as well as the biomass specific growth rate, shall be kept constant. The system behavior for varying sugar concentrations in the SSL is examined by supplementing and dissolving additional sugars in the feed. The different phases of the fermentation and the needed control actions are planned and simulated in section 7.1. The measurements obtained from the experimental run are plotted in section 7.2.

7.1 Experimental planning

The fermentation can be separated into four phases. The **extended batch** in the first 48 hours of the process is started with one liter batch media. After 18 and 26 hours, additional media is added so that the reactor volume is doubled at each step. The batch phase is followed by the **deacellerostat** and a **stabilizing phase**, where the cell retention is started. The **continuous phase** is started subsequently. The timeline of the different phases can be found in Table 7.1.

During the continuous phase, the SSL media is supplemented with additional glucose and mannose in order to obtain an understanding on the process behaviour for varying feed concentrations resulting in the concentration profile displayed in Figure 7.1.

Table 7.1: Timeline of fermentation phases. The fermentation can be separated into four phases. During the extended batch phase, the deacellerostat and the stabilizing phase, media is added to the process with predefined trajectories based on simulations to obtained the desired system behavior. The procedure is analog for harvest and bleed rate. During the continuous phase, the feed, harvest and bleed rates are set dynamically.

	Starting time of phase after process start	Duration of phase
Extended Batch	0 hours	48 hours
Deacellerostat	48 hours	24 hours
Stabilizing phase	72 hours	18 hours
Continuous phase	90 hours	´200+ hours

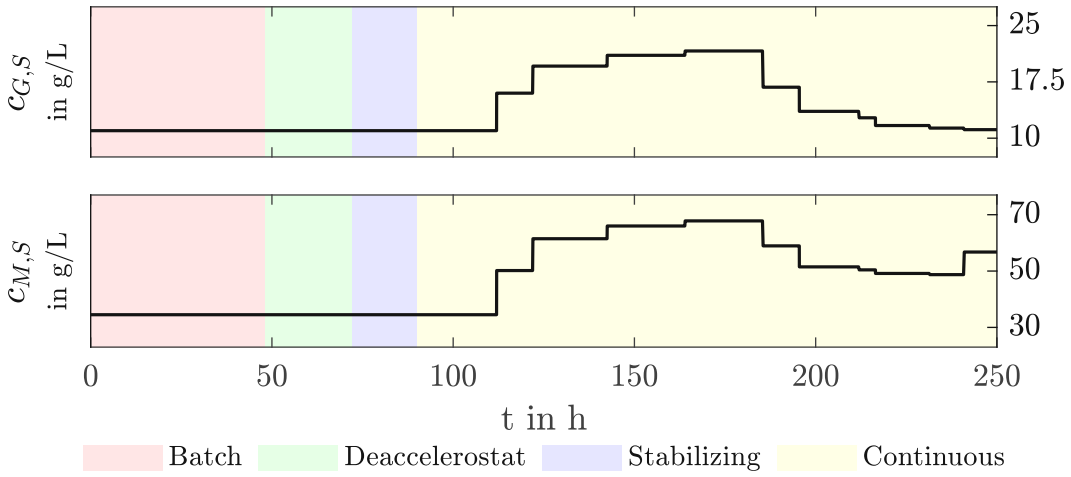

Figure 7.1: Experimental planning - concentration profile of SSL feed. During the continuous phase SSL is supplemented with glucose and mannose to obtain varying concentrations during the process. By adapting the feed, harvest and bleed rates, the process is kept in a stable state.

In the first three phases of the process, the applied feed, harvest and bleed rates are predefined. During the continuous phase, the rates are calculated by the controller so that the desired setpoints of the outputs are reached. The expected system behaviour is plotted in Figure 7.2 which is achieved by the predefined and calcu-

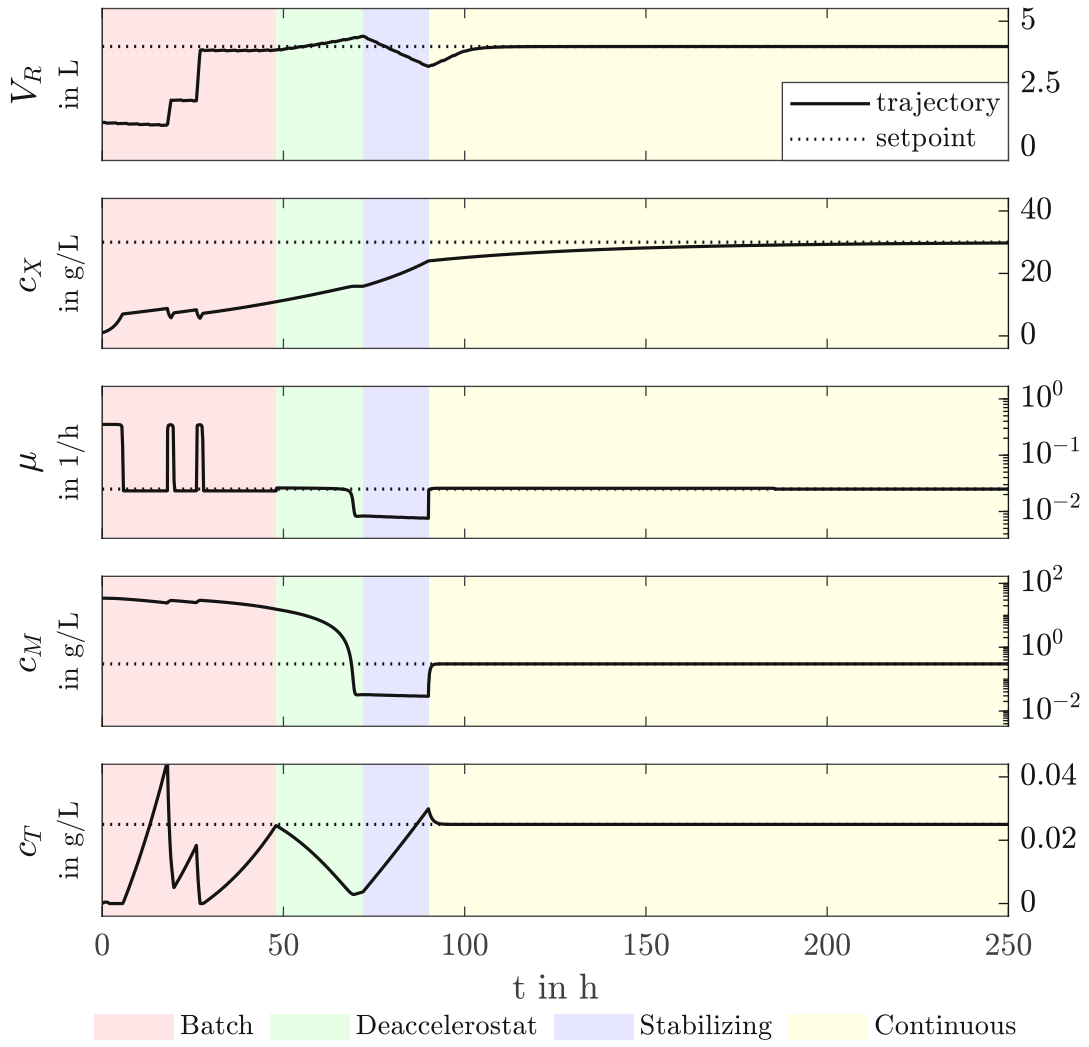

Figure 7.2: Experimental planning - output trajectories for the four experimental phases. The simulated system behaviour (black line) for the different phases is displayed. During the batch, deaccelerostat and stabilizing phase the process is started up. A stable state with the desired setpoints (dotted line) can be reached and maintained during the continuous phase.

lated rates in Figure 7.3. Nutrients are added by an exponential trajectory for $\dot{V}_N$ during the batch phase. The transition from the extended batch phase, which is characterised by high sugar concentrations, low biomass concentrations as well as uncontrolled and maximal biomass specific growth rates, to the continuous phase with low sugar concentrations, high biomass concentrations and controlled biomass

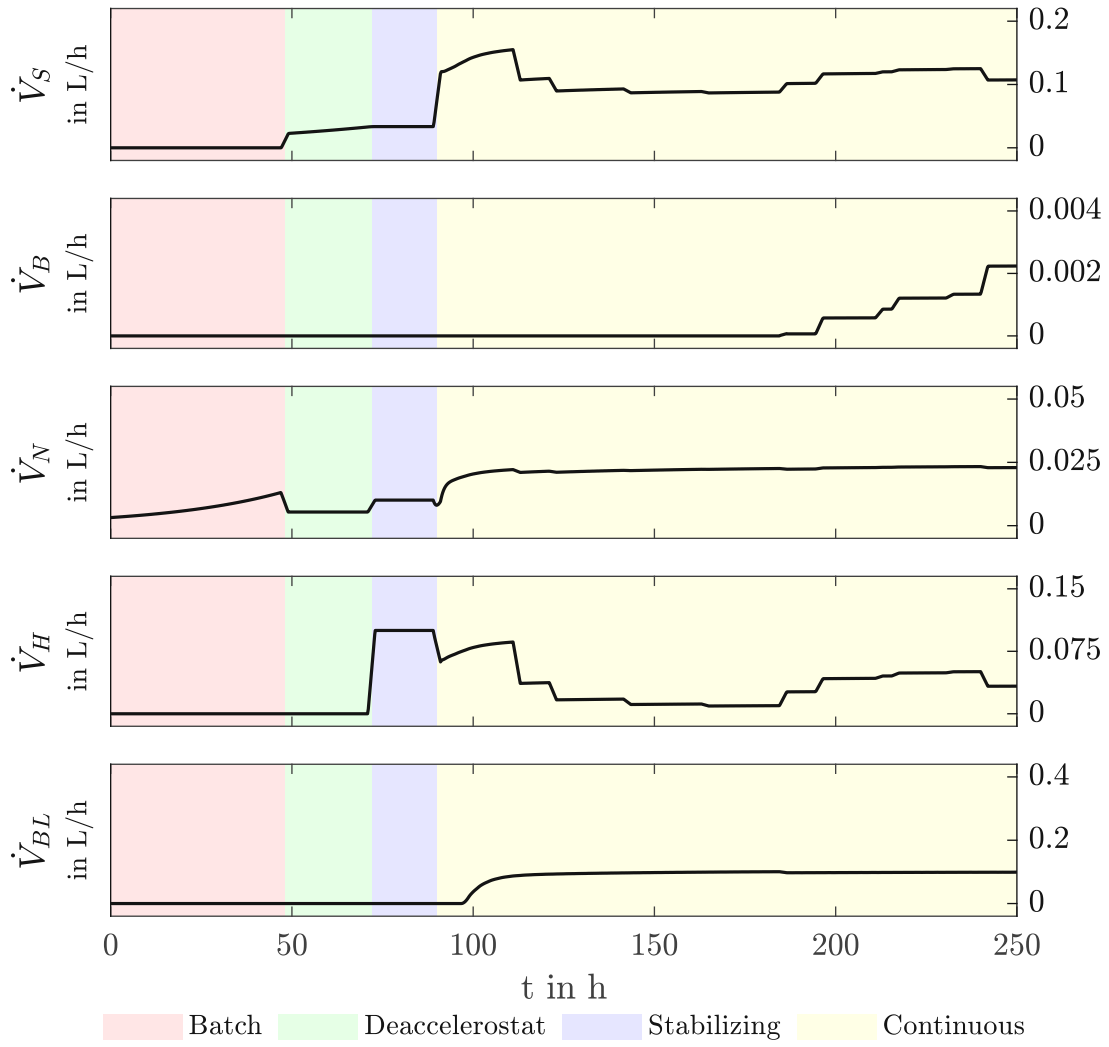

Figure 7.3: Experimental planning - volumetric flows for the four experimental phases. The predefined (batch, deaccelerostat, stabilizing phase) and calculated (continuous phase) feed, harvest and bleed rates are plotted. By varying rates during the continuous phase, variations of the sugar concentrations in the SSL can be accounted for.

growth, is done by the deacellerostat and the stabilizing phase. SSL and nutrients are added with predefined feed rates. After 72 hours, the stabilizing phase is started and the cell retention is turned on. The biomass concentration increases further. 90 hours after inoculation, the continuous phase is started. Feed, bleed and harvest rates are calculated by the control algorithm and send to the corresponding pumps.

7.2 Results from experimental run

In the following, the results of the experiment controlled with the feedforward strategy are presented, analyzed and discussed. The expected values from simulation and measured data of the experimental run are compared. In Figure 7.4, the glucose and mannose concentration profiles in the SSL can be seen. The expected and measured courses are almost identically.

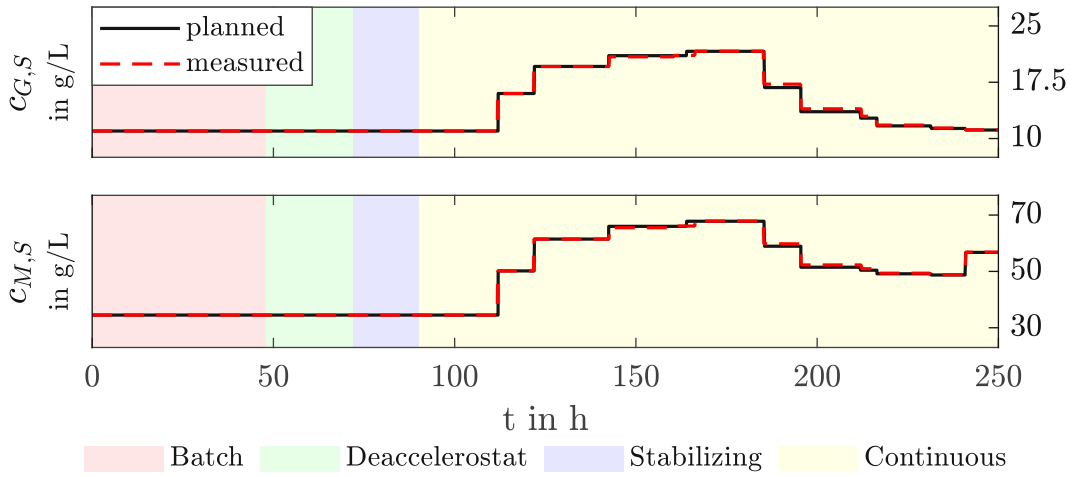

Figure 7.4: Experimental data - concentration profile of SSL feed. The measured (red) concentration profiles for glucose and mannose in the SSL are almost identical to the planned (black) course.

The measurements of the reactor volume, the mannose concentration in the broth and the OUR and CER are plotted in Figure 7.5. Clogging of harvest and bleed pipes led to a considerable deviation of the reactor volume from the expected course. If these can be eliminated, a constant reactor volume during the continuous phase can be obtained. However, the measured mannose concentrations deviate considerably from the simulated values, which is also reflected in the offgas signals, suggesting considerable model-plant mismatch. Further parameter optimisation and the inclusion of the consumption of other sugars present in the media could lead to a better model and therefore to an improved process understanding. Nevertheless, OUR and CER signals with small fluctuations around a constant level starting at 150 hours suggest that the process transitioned to a stable and continuous phase.

Using the continuous measurements of the weights of the storage tanks for SSL, BALI, nutrients, harvest and bleed as well as their densities, the feed, harvest and bleed

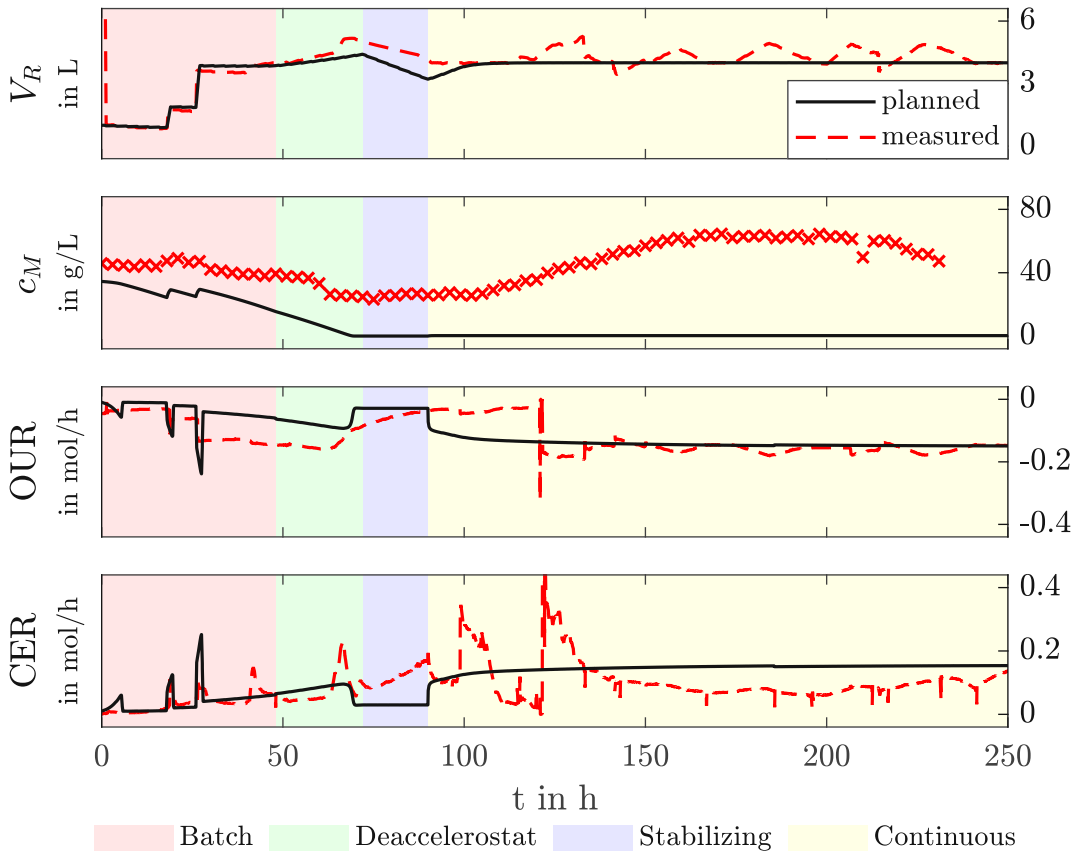

Figure 7.5: Experimental data - output trajectories. The measured (red) and planned (black) signals are compared. (V_R) Clogging of the bleed pipes led to deviations from the reactor volume setpoint. (c_M) Significant deviations from the calculated course suggest considerable model-plant mismatch. Small changes in the maximal mannose uptake rate lead to significant accumulation of mannose in the broth as shown in chapter 6. Further experiments for improved parameter fit should be considered. (OUR, CER) Despite the considerable model-plant mismatch, constant signals after 150 hours were obtained suggesting that the process was in a continuous phase.

rates are calculated (Figure 7.6). Considerable differences from the desired rates can be seen. The SSL feed was adjusted well. Due to the very low feed rates, the BALI™ feed could not be adjusted accurately. By using a pump for smaller pumping rates, the addition of the BALI™ feed can be improved. The nutrient feed was added with sufficient accuracy, especially in the continuous phase, as no limitation and

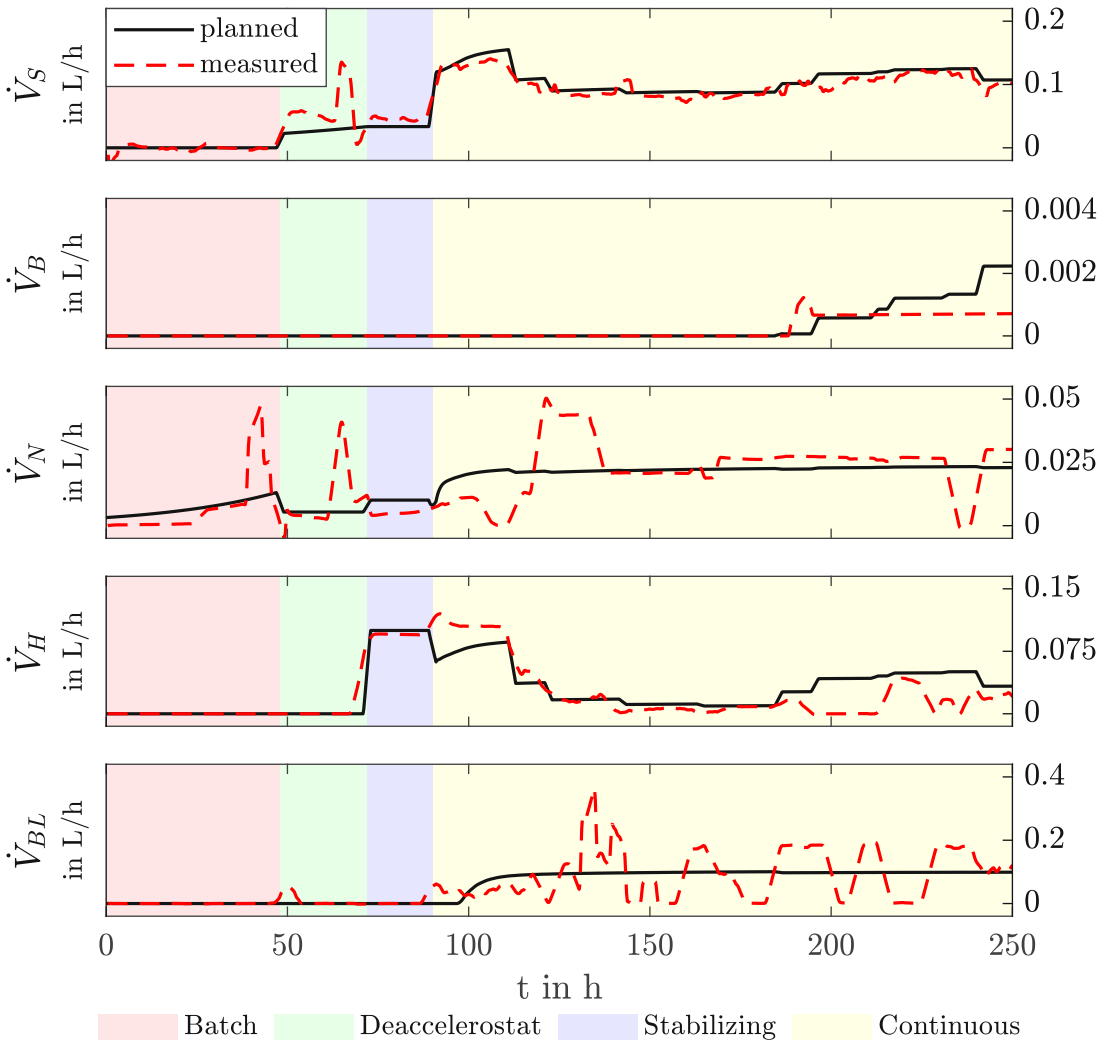

Figure 7.6: Experimental data - volumetric flows. Significant deviations from the planned (black) feed, harvest and bleed rates are observed during the experimental run (red). SSL and nutrition feed was added with sufficient accuracy. The very small feed rates of BALI™ were not added accurately. Due to sedimentation and clogging in the harvest and bleed pipes, the rates dropped periodically.

immoderate precipitation was observed during the process. Problems with clogging occurred both in the harvest and bleed pipes resulting in rates periodically close to zero. Larger piping and periodic flushing should minimize sedimentation and clogging. The proposed minimal changes are expected to resolve problems with accuracy of feed addition and harvesting.

Chapter 8

Discussion

A new fermentation process for *C. glutamicum* with two independent alternative carbon sources including a MIMO model-based control strategy was established. The valorization of two lignocellulosic waste streams from the paper and pulp industry as secondary raw materials for bioprocessing was shown. Establishment of the process can contribute to an overall circular economy by reducing waste and pollution. However further research for both the process and the control strategy are needed to ensure stable and economic processes.

C. glutamicum has shown its potential as expression host by consuming different sugars available in the added carbon sources. Despite being not genetically modified for improved mannose consumption, the used wild strain has shown promising results. The parameter analysis showed that for an increased maximal mannose uptake $q_{M,max}$, the harvest rates as well as time-space yield can be significantly increased. Consequently, examination of strains with improved mannose consumption is of high interest.

The challenge of varying concentrations in the complex and recycled media is tackled by adding two different carbon sources with federates calculated by the model-based control strategy. It was shown, that by using the method of feedback linearization, changes in the media composition are compensated proactive and the process can be maintained in a stable state. Due to the fact that SSL is added as the main carbon source, changes in the SSL influence the process significantly. By developing real-time analysis strategies for measuring the varying sugar concentration in the feeds, the feeds, harvest and bleed rates can be adjusted by the obtained feedback linearized control law.

In the feasibility study it was shown that due to the coupling of the states, the choice of a single setpoint can not be done independently of the other setpoints. With

the feasibility space that considers the chemical and physical limits of the system, beneficial setpoint combinations can be identified. By adapting the setpoints for the biomass concentration and the specific biomass growth rate, the ratio between harvest and bleed rate can be adjusted. Adaptations of the setpoints for the specific growth rate and the mannose concentrations changes the ratio of added SSL and BALI™.

By simulating the system behavior with deviating process parameters, the examined control strategies were compared. With increasing knowledge over the system, the control errors were reduced. However, measurement expenses increase. Promising results for the estimation of the biomass concentration, the specific biomass growth rate and the nutrient concentration are obtained suggesting that the process can be controlled with small control errors while minimizing measurement expenses. Due to relatively large estimation errors for the mannose concentration as suggested for MPC3, measurements of the mannose concentration in the broth is of interest for the control action. However compared to the control errors for the mannose concentration obtained by the experiment with feedforward control, a significant improvement with MPC3 is expected.

Despite the promising results obtained both from simulation and the experimental run, considerable model-plant mismatch was observed. The kinetic parameters from [2] were fitted to measurements from experiments with full defined medium supplemented with SSL as sole carbon source. During the conducted experiment, the culture was grown on pure diluted SSL utilizing existing amounts of vitamins and trace elements present in the SSL from the pulp mill process to decrease media costs and increase sustainability. Only compounds that were found to be not present in sufficient quantities were added separately by the nutrient feed. Consequently, further experiments for both parameter fitting and improvement of control strategy are of interest. Including a kinetic description of additional components available in the SSL and BALI™, such as acetate and xylose, could further improve process understanding and control accuracy.

As shown in the first experimental run, the process was successfully controlled and a continuous process was obtained with feedforward control. By including feedback from the plant in the control algorithm further improvement of the process control can be expected. For MPC1 with the highest measurement expenses, major adaptations of the experimental setup have to be performed and analytical methods for online measurement of the biomass and nutrient concentration have to be established. For MPC2, the measuring procedure for the glucose and mannose concentration in the broth has to be automated to provide reliable feedback signals with constant

sampling frequency. MPC3 can be implemented and tested for process control with the current experimental setup as all measurement signals needed are taken with sufficient sampling frequency.

However, significant improvements in process understanding and process control can be expected through further steps in process monitoring, modelling, optimization and automation. Improving the control algorithm for multi-rate measurement signals can further improve the control action and reduce the problem introduced due to the omnipresent difficulties of measuring broth concentrations in bioprocessing. As shown for the different measurement scenarios, including further information obtained during the process improves process control and reduces control errors.

By simulating the system behavior in the different phases of the experiment with the planned feedrates, it was possible to show, how the process must be controlled so that a stable state can be reached. The combination of the four experimental phases, namely the batch phase, the deaccelerostat, the stabilizing phase and the continuous phase, showed, what different measures have to be taken in order to achieve a stable and beneficial state of the process for the given experimental setup.

Chapter 9

Conclusion

In this thesis, a model-based control strategy for a *multiple input, multiple output* system was developed and analysed. It was shown that the continuous bioprocess with cell retention can be controlled and a stable state can be reached by adapting the five input variables, namely the harvest rate, the bleed rate, a nutrient solution and the two alternative carbon sources SSL and BALI™, two waste water streams from the pulping industry. Recycling by- and waste products from established processes as secondary raw materials a contribution to an overall circular economy by enabling ecological and environmental friendly production processes is made. However, due to the complex composition of the waste water streams, bioprocessing is challenging and advanced control strategies are needed. By the method of feedback linearization a control strategy was found, where all nonlinearities of the model are considered. A stable state with constant volume and constant concentrations in the reactor was reached and maintained. Varying concentrations in the feed were accounted for in a proactive way by adaptation of the feed, harvest and bleed rates.

Despite the physical and biochemical limits of the process, the high flexibility and potential of the control of the bioprocess was shown. Beneficial setpoint combinations were identified in the feasibility study under the assumption of a perfect model. The influence of changing kinetic parameters, feed concentrations and setpoints was examined. For feedforward control, it was shown that for varying parameters a stable state can be reached. The control action was further improved with the suggested MPC. The influence of different measurement scenarios was examined.

The high potential of the suggested process and control strategy was shown by the data obtained from the experimental run. However, significant model-plant mismatch was observed. Additional experiments to improve the model structure and parameter fit are needed. An improvement of the setup for further experiments was discussed.

To summarize, the promising results from simulations and first experimental run, a limited number of publications on the control of bioprocesses with multiple carbon sources, the overall demand for good process understanding, which is based on model-based approaches, and possible positive effects on waste management and environment, ask for further studies regarding the suggested control strategy in order to design an ecological, stable, resource efficient and overall beneficial process.

Appendix A

Mathematical definitions

Diffeomorphism

A diffeomorphism is an unambiguous function that is continuously differentiable and whose inverse is also continuously differentiable, meaning

$$\boldsymbol{z} = \boldsymbol{t}(\boldsymbol{x}) \tag{A.1}$$

$$\boldsymbol{x} = \boldsymbol{t}^{-1}(\boldsymbol{z}) = \boldsymbol{t}^{-1}(\boldsymbol{t}(\boldsymbol{x})). \tag{A.2}$$

The inverse function $\boldsymbol{t}^{-1}(\boldsymbol{x})$ exists, if the Jacobian matrix $\frac{\partial \boldsymbol{t}(\boldsymbol{x})}{\partial \boldsymbol{x}}$ is non-singular.

Lie derivative

The derivative of a scalar function $\lambda(\boldsymbol{x})$ along a vector field $\boldsymbol{a}(\boldsymbol{x})$ is defined by

$$L_{\boldsymbol{a}}\lambda = \frac{\partial(\lambda(\boldsymbol{x}))}{\partial \boldsymbol{x}}\boldsymbol{a}(\boldsymbol{x}) = \mathrm{grad}^T\lambda(\boldsymbol{x})\boldsymbol{a}(\boldsymbol{x}). \tag{A.3}$$

Note that $\mathbb{R}^n \to \mathbb{R}$. Furthermore, the following applies

$$L^0_{\boldsymbol{a}}\lambda = \lambda(\boldsymbol{x}) \tag{A.4}$$

and

$$L^i_{\boldsymbol{a}}\lambda = \frac{\partial(L^{i-1}_{\boldsymbol{a}}\lambda)}{\partial \boldsymbol{x}}\boldsymbol{a}(\boldsymbol{x}). \tag{A.5}$$

Bibliography

[1] P. Sinner, M. Stiegler, C. Herwig, and J. Kager. Noninvasive online monitoring of corynebacterium glutamicum fed-batch bioprocesses subject to spent sulfite liquor raw material uncertainty. *Bioresource technology*, 321:124395, 2021.

[2] P. Sinner, J. Kager, S. Daume, and C. Herwig. Model-based analysis and optimisation of a continuous corynebacterium glutamicum bioprocess utilizing lignocellulosic waste. *IFAC PapersOnLine*, 52-26:181–186, 2019.

[3] D. Das and S. Pandit. *Industrial biotechnology*. CRC Press, Boca Raton, FL, first edition edition, 2021.

[4] L. C. Vitorino and L. A. Bessa. Technological microbiology: Development and applications. *Frontiers in microbiology*, 8:827, 2017.

[5] D. Kiefer, M. Merkel, L. Lilge, R. Hausmann, and M. Henkel. High cell density cultivation of corynebacterium glutamicum on bio-based lignocellulosic acetate using ph-coupled online feeding control. *Bioresource technology*, 340:125666, 2021.

[6] R. Kutscha and S. Pflügl. Microbial upgrading of acetate into value-added products-examining microbial diversity, bioenergetic constraints and metabolic engineering approaches. *International journal of molecular sciences*, 21(22), 2020.

[7] Z. Usmani, M. Sharma, A. K. Awasthi, N. Sivakumar, T. Lukk, L. Pecoraro, V. K. Thakur, D. Roberts, J. Newbold, and V. K. Gupta. Bioprocessing of waste biomass for sustainable product development and minimizing environmental impact. *Bioresource technology*, 322:124548, 2021.

[8] P. Fatehi and Y. Ni. Integrated forest biorefinery – sulfite process. In J. Zhu, X. Zhang, and X. Pan, editors, *Sustainable Production of Fuels, Chemicals, and Fibers from Forest Biomass*, volume 1067 of *ACS Symposium Series*, pages 409–441. American Chemical Society, Washington, DC, 2011.

[9] H. G. Lawford and J. D. Rousseau. Production of ethanol from pulp mill hardwood and softwood spent sulfite liquors by genetically engineered e. coli. *Appl Biochem Biotechnol*, 39-40:667–685, 1993.

[10] G. Rødsrud, M. Lersch, and A. Sjöde. History and future of world's most advanced biorefinery in operation. *Biomass and Bioenergy*, 46:46–59, 2012.

[11] P. Sinner, M. Stiegler, O. Goldbeck, G. M. Seibold, C. Herwig, and J. Kager. Online estimation of changing metabolic capacities in continuous corynebacterium glutamicum cultivations growing on a complex sugar mixture. *Biotechnology and bioengineering*, 2021.

[12] J. Becker, C. M. Rohles, and C. Wittmann. Metabolically engineered corynebacterium glutamicum for bio-based production of chemicals, fuels, materials, and healthcare products. *Metabolic engineering*, 50:122–141, 2018.

[13] H. Narayanan, M. F. Luna, M. von Stosch, Mariano N. Cruz B., G. Polotti, M. Morbidelli, A. Butté, and M. Sokolov. Bioprocessing in the digital age: The role of process models. *Biotechnology journal*, 15(1):e1900172, 2020.

[14] A. S. Rathore, S. Mishra, S. Nikita, and P. Priyanka. Bioprocess control: Current progress and future perspectives. *life*, 11(6):557, 2011.

[15] G. D. Iyovo and G. Du. Sustainable bioenergy bioprocessing: Biomethane production, digestate as biofertilizer and as supplemental feed in algae cultivation to promote algae biofuel commercialization. *Journal of Microbial & Biochemical Technology*, 02(04):100–106, 2010.

[16] P. A. López Pérez, R. A. Lopez, and Alejandro R. Femat F. *Control in bioprocessing: Modeling, estimation and the use of soft sensors*. Wiley, Hoboken NJ USA, first edition edition, 2020.

[17] R. Aguilar-López and I. Neria-González. Controlling continuous bioreactor via nonlinear feedback: modelling and simulations approach. *Bulletin of the Polish Academy of Sciences Technical Sciences*, 64(1):235–241, 2016.

[18] M. A. Henson and D. E. Seborg. Nonlinear control strategies for continuous fermenters. *Chemical Engineering Science*, 47(4):821–835, 1992.

[19] T. Pröll and N. M. Karim. Nonlinear control of a bioreactor model using exact and i/o linearization. *International Journal of Control*, 60(4):499–519, 1994.

[20] Z.-Q. Wang, S. Skogestad, and Y. Zhao. Extract linearization control of continuous bioreactors: a comparison of various control structures. In *Proceedings of IEEE International Conference on Control and Applications*, pages 107–112.

IEEE, 13-16 Sept. 1993.

[21] F. Angulo, R. Munoz, and G. Olivar. Control of a bioreactor using feedback linearization. In *2007 Mediterranean Conference on Control & Automation*, pages 1–6. IEEE, 27.06.2007 - 29.06.2007.

[22] R. Aguilar-López. Input-output linearizing-type controller design with application to continuous bioreactor. *Comptes rendus de l'Académie bulgare des Sciences*, 70(3):321–328, 2017.

[23] M. Abadli, L. Dewasme, S. Tebbani, D. Dumur, and A. Vande Wouwer. Generic model control applied to e. coli bl21(de3) fed-batch cultures. *Processes*, 8(7):772, 2020.

[24] J. Zietkiewicz. Linear quadratic control with feedback-linearized models. *STUDIA Z AUTOMATYKI I INFORMATYKI*, 40, 2015.

[25] A. Kugi. *Regelungssysteme 2*. TU Wien - Insitut für Automaisierungs- und Regelungstechnik, Vienna, 2021.

[26] N. C. Shaner, R. E. Campbell, P. A. Steinbach, B. N. G. Giepmans, A. E. Palmer, and R. Y. Tsien. Improved monomeric red, orange and yellow fluorescent proteins derived from discosoma sp. red fluorescent protein. *Nature biotechnology*, 22(12):1567–1572, 2004.

[27] K. Schügerl and K.-H. Bellgardt. *Bioreaction Engineering*. Springer Berlin Heidelberg, Berlin, Heidelberg, 2000.

[28] M. Aehle, A. Kuprijanov, S. Schaepe, R. Simutis, and A. Lübbert. Simplified off-gas analyses in animal cell cultures for process monitoring and control purposes. *Biotechnology letters*, 33(11):2103–2110, 2011.

[29] S. Jakubek, A. Schirrer, and O. König. *Adaptive and Predictive Control*. Technische Univeristät Wien - Institut für Mechanik und Mechatronik, Vienna, 2019.